Robotica (2017) volume 35, pp. 310–336. © Cambridge University Press 2015
doi:10.1017/S026357471500051X

Uncertainty estimation in robust tracking control of robot manipulators using the Fourier series expansion

Saeed Khorashadizadeh* and Mohammad Mehdi Fateh

Department of Electrical and Robotic Engineering, Shahrood University, 361995161 Shahrood, Iran

(Accepted May 23, 2015. First published online: July 20, 2015)

SUMMARY

This paper presents a novel control algorithm for electrically driven robot manipulators. The proposed control law is simple and model-free based on the voltage control strategy with the decentralized structure and only joint position feedback. It works for both repetitive and non-repetitive tasks. Recently, some control approaches based on the uncertainty estimation using the Fourier series have been presented. However, the proper value for the fundamental period duration has been left as an open problem. This paper addresses this issue and intuitively shows that in order to perform repetitive tasks; the least common multiple (LCM) of fundamental period durations of the desired trajectories of the joints is a proper value for the fundamental period duration of the Fourier series expansion. Selecting the LCM results in the least tracking error. Moreover, the truncation error is compensated by the proposed control law to make the tracking error as small as possible. Adaptation laws for determining the Fourier series coefficients are derived according to the stability analysis. The case study is an SCARA robot manipulator driven by permanent magnet DC motors. Simulation results and comparisons with a voltage-based controller using adaptive neuro-fuzzy systems show the effectiveness of the proposed control approach in tracking various periodic trajectories. Moreover, the experimental results on a real SCARA robot manipulator verify the successful practical implementation of the proposed controller.

KEYWORDS: Robot manipulators; Voltage control strategy; Fourier series expansion; Uncertainty estimation; Robust tracking control.

1. Introduction

Over the past decades, the problem of robust tracking control of robot manipulators has been the focus of considerable research studies.[1–4] Establishing an exact mathematical model for designing a model-based controller is a difficult task, since robot manipulators are complex nonlinear multivariable systems with structured and unstructured uncertainties.[1–4] Therefore, nominal models have been recommended for robust and adaptive control approaches.[1–4] Usually, the proposed nominal models have the same structures as the actual models. Consequently, the lengthy and tedious regressor analysis is inevitable in the traditional robust and adaptive control methodologies,[1–4] since these approaches are based on the linear parameterization of the manipulator dynamics. Sometimes, obtaining a suitable nominal model requires offline identification.[1–4] Sensing requirement is another challenge in this field.[5] Most of presented algorithms need the velocity feedbacks and some of them require the acceleration feedbacks. Also, motor currents and their time derivatives may be required.[6] These signals are usually contaminated with noise and may degrade the controller performance. Moreover, many commercial robots provide the user with only joint position measurements. Thus, practical implementation of these controllers may be impossible or too expensive. These reasons are why the identification is not used in this paper.

* Corresponding author. E-mail: s_khorashadi@yahoo.com

https://doi.org/10.1017/S026357471500051X Published online by Cambridge University Press

To solve these problems, some observer–controller structures have been proposed[7–9] in which these un-measurable signals are estimated. However, these approaches increase the computational burden of the controller by augmenting the observer dynamics. Moreover, in these approaches, it has been assumed that the lumped uncertainty is constant or varies slowly. This assumption can be violated easily in the applications where high speeds are needed.

Sliding mode control (SMC),[10] as a robust control strategy, is very simple and popular. However, the uncertainty upper bound should be known in advance or estimated in SMC. If the estimated bound is greater than its actual value, the control system will face saturation of input and the chattering phenomenon, while too low estimation of the bounds may cause a higher tracking error.[5] Parameter estimation and upper bounding adaptation have been effectively used in adaptive-robust control approaches for robot manipulators.[11]

Nowadays, various neural networks and fuzzy systems are extensively applied in the field of robot control.[12–16] The universal approximation property and linear parameterization are the most important motivations for these widespread applications. Fault-tolerance, parallelism and excellent learning capabilities are other beneficial characteristics of fuzzy systems and neural networks. The unknown parameters in the neural networks structures and fuzzy systems are adjusted online using some adaptation laws derived from the Lyapunov-based stability analysis. Besides the aforementioned advantages, there are some disadvantages in applying artificial intelligence to control systems. For instance, in order to make the parameters of neural networks and fuzzy systems limited to pre-defined regions, the projection algorithm is needed[17] which can impose additional computational burden to the processor. Sometimes, designing a satisfactory fuzzy controller for a complicated system requires the knowledge of some experts specialized in that field.[17] Without this vital information, designing a proper fuzzy controller may be a tedious task due to the time-consuming trial and error procedure. Moreover, fuzzy and neural estimators require various feedbacks for their inputs. For example, if the uncertainty is a function of some state variables, all those states should be available and fed to the fuzzy system or neural network as inputs.

Most of robust approaches in the field of robot control are based on the torque control strategy (TCS). In this strategy, the control law computes the desired torques which should be applied to the robot joints. The actuator dynamics is excluded in this strategy, whereas the computed torque cannot be applied to the manipulator without actuators such as electrical motors. Thus, there is a question that how the actuator input (motor voltage) should be excited. To solve this problem, some voltage-based approaches have been presented.[18–22]

Recently, regressor free control of robot manipulators has been presented[23,24] which is based on function approximation techniques. In this approach, uncertainties such as the inertia matrix, Jacobian matrix or gravity vector have been estimated using Fourier series. It should be emphasized that the fundamental period duration and the number of used frequencies are important parameters which considerably influence the controller performance. Certainly, increasing the number of terms in the Fourier series will make the approximation error smaller. On the other hand, hardware limitations such as available memory space will not permit arbitrary increasing of the Fourier series terms. To achieve a satisfactory trade-off between hardware limitations and accuracy, the Fourier series terms should be selected carefully.

In this study, based on the function approximation ability of Fourier series, a robust control design for electrically driven robot manipulators is developed and simulated. The proposed control law is model-free based on the voltage control strategy[18] (VCS) with the decentralized structure and only joint position feedback. It works for both repetitive and non-repetitive tasks. It works for both repetitive and non-repetitive tasks. To perform repetitive tasks, it is explained that the least common multiple of the fundamental period durations of desired trajectories is a suitable selection for fundamental period duration of the Fourier series expansion according to the robotic system characteristics. Moreover, the truncation error is compensated in the control law. In comparison with observer–controller structures,[7–9] the proposed method is superior, since there is no need to assume that the uncertainties vary slowly. Reducing the number of feedbacks from different state variables and tuning parameters and also eliminating the need for expert knowledge are advantages of the proposed controller in comparison with adaptive fuzzy or neural approaches.[12–16] Conventional robust controllers[1–6] require nominal models, while the proposed control law is model-free. Some practical problems should be discussed related to the use of motors, drives and gears. The robotic system used in this paper has equipped by the geared DC motor. The motors were considered;

https://doi.org/10.1017/S026357471500051X Published online by Cambridge University Press

however, the dynamics of drivers were ignored since its dynamics are much faster than the dynamics of manipulator and motors. In contrast, the majority of control approaches of robot manipulator in the literature are based on the TCS in those the dynamics of motors and drivers are ignored.

The paper is organized into eight sections. Following Introduction, in Section 2, function approximation using Fourier series is described. Section 3 explains the mathematic model of electrically driven robot manipulators. Section 4 presents the proposed control law. The stability analysis is given in Section 5. The proper value of period duration of Fourier series is determined in Section 6. Simulation and experimental results are presented in Section 7 and 8, respectively. Finally, Section 9 concludes the paper.

2. Function Approximation using Fourier Series

Uncertainty estimators are not confined to fuzzy systems and neural networks. It is well known that Fourier series can approximate periodic functions. A non-periodic function defined in limited time interval is assumed to be repeated; thereby it can be expanded by a Fourier series. According to Kreyszig,[25] if the function $g(t)$ defined on $[t_1, t_2]$ satisfies Dirichlet's conditions, then it can be expressed as

$$g(t) = a_0 + \sum_{k=1}^{\infty} a_k \cos(\omega_k t) + b_k \sin(\omega_k t) \tag{1}$$

$$a_0 = \frac{1}{T}\int_{t_1}^{t_2} g(t)dt \tag{2}$$

$$a_k = \frac{2}{T}\int_{t_1}^{t_2} f(t)\cos\left(\frac{2k\pi}{T}t\right)dt \tag{3}$$

$$b_k = \frac{2}{T}\int_{t_1}^{t_2} f(t)\sin\left(\frac{2k\pi}{T}t\right)dt \tag{4}$$

where a_0, a_k and b_k are the Fourier series coefficients and $T = t_2 - t_1$ is the fundamental period of $g(t)$ and $\omega_k = 2k\pi/T$. The truncation error is defined as

$$\varepsilon_m(t) = g(t) - g_m(t) \tag{5}$$

where $g_m(t) = a_0 + \sum_{k=1}^{m} a_k \cos(\omega_k t) + b_k \sin(\omega_k t)$ is the Fourier series approximation. Note that $g_m(t)$ can be written as

$$g_m(t) = P^T \xi(t) \tag{6}$$

in which

$$P = \begin{bmatrix} a_0 & a_1 & b_1 & \ldots & a_m & b_m \end{bmatrix}^T \tag{7}$$

and

$$\xi(t) = \begin{bmatrix} 1 & \cos(\omega_1 t) & \sin(\omega_1 t) & \ldots & \cos(\omega_m t) & \sin(\omega_m t) \end{bmatrix}^T \tag{8}$$

Remark 1 It should be mentioned that in control systems, the function $g(t)$ is not available and (2)–(4) cannot be applied for calculation of the Fourier series coefficients. In fact, these coefficients should be adjusted online using adaptation laws derived from the stability analysis.

https://doi.org/10.1017/S026357471500051X Published online by Cambridge University Press

3. Modeling

The dynamic model of a robot manipulator can be described by n generalized coordinates representing the degrees-of-freedoms of the n joints as[26]

$$\mathbf{D}(\mathbf{q})\ddot{\mathbf{q}} + \mathbf{C}(\mathbf{q}, \dot{\mathbf{q}})\dot{\mathbf{q}} + \mathbf{G}(\mathbf{q}) = \tau_{\mathbf{l}} \tag{9}$$

where $\mathbf{q} \in R^n$ is the vector of joint positions, $\mathbf{D}(\mathbf{q})$ the $n \times n$ matrix of manipulator inertia, $\mathbf{C}(\mathbf{q}, \dot{\mathbf{q}})\dot{\mathbf{q}} \in R^n$ the vector of centrifugal and Coriolis torques, $\mathbf{g}(\mathbf{q}) \in R^n$ the vector of gravitational torques and $\boldsymbol{\tau}_{\mathbf{l}} \in R^n$ the joint torque vector of robot. The electric motors provide the joint torque vector as follows:

$$\mathbf{J_m}\ddot{\mathbf{q}}_{\mathbf{m}} + \mathbf{B_m}\dot{\mathbf{q}}_{\mathbf{m}} + \mathbf{r}\boldsymbol{\tau}_{\mathbf{l}} = \boldsymbol{\tau}_{\mathbf{m}} \tag{10}$$

where $\boldsymbol{\tau}_{\mathbf{m}} \in R^n$ is the torque vector of motors, $\mathbf{J_m}$, $\mathbf{B_m}$, and $\mathbf{r}$ are the $n \times n$ diagonal matrices for motor coefficients namely the inertia, damping, and reduction gear, respectively. The joint velocity vector $\dot{\mathbf{q}}$ and the motor velocity vector $\dot{\mathbf{q}}_{\mathbf{m}} \in R^n$ are related through the gears to yield

$$\mathbf{r}\dot{\mathbf{q}}_{\mathbf{m}} = \dot{\mathbf{q}}. \tag{11}$$

In order to obtain the motor voltages as the inputs of system, we consider the electrical equation of geared permanent magnet DC motors in the matrix form

$$\mathbf{RI_a} + \mathbf{L}\dot{\mathbf{I}}_{\mathbf{a}} + \mathbf{K_b}\mathbf{r}^{-1}\dot{\mathbf{q}} = \mathbf{v} \tag{12}$$

where $\mathbf{v} \in R^n$ is the vector of motor voltages and $\mathbf{I_a} \in R^n$ is the vector of motor currents. $\mathbf{R}$, $\mathbf{L}$ and $\mathbf{K_b}$ represent the $n \times n$ diagonal matrices for the coefficients of armature resistance, inductance, and back-emf constant, respectively. The motor torque vector $\boldsymbol{\tau}_{\mathbf{m}}$ as the input for dynamic (10) is produced by the motor current vector

$$\mathbf{K_m}\mathbf{I_a} = \boldsymbol{\tau}_{\mathbf{m}} \tag{13}$$

where $\mathbf{K_m}$ is a diagonal matrix of the torque constants. Using (9)–(13), the state-space model is obtained

$$\dot{\mathbf{x}} = \mathbf{F}(\mathbf{x}) + \mathbf{bv} \tag{14}$$

in which

$$\mathbf{x} = \begin{bmatrix} \mathbf{q} & \dot{\mathbf{q}} & \mathbf{I_a} \end{bmatrix}^T, \mathbf{b} = \begin{bmatrix} \mathbf{0} & \mathbf{0} & \mathbf{L}^{-1} \end{bmatrix}^T \tag{15}$$

$$\mathbf{F}(\mathbf{x}) = \begin{bmatrix} \mathbf{x}_2 \\ (\mathbf{J}\mathbf{r}^{-1} + \mathbf{r}\mathbf{D}(\mathbf{x}_1))^{-1}(-(\mathbf{B}\mathbf{r}^{-1} + \mathbf{r}\mathbf{C}(\mathbf{x}_1, \mathbf{x}_2))\mathbf{x}_2 - \mathbf{r}\mathbf{G}(\mathbf{x}_1) + \mathbf{K_m}\mathbf{x}_3) \\ -\mathbf{L}^{-1}(\mathbf{K_b}\mathbf{r}^{-1}\mathbf{x}_2 + \mathbf{R}\mathbf{x}_3) \end{bmatrix} \tag{16}$$

4. Proposed Control Law

We can design the controller based on nominal models.[15] However, it requires the nominal values of $\hat{\mathbf{R}}$, $\hat{\mathbf{K}}_{\mathbf{b}}$ and $\hat{\mathbf{r}}$. Moreover, feedbacks from motor currents are necessary. In this paper, we assume that these nominal values are not available.[16] Thus, in order to eliminate the need for nominal model and feedbacks from motor currents, we can consider (12) as

$$\dot{\mathbf{q}} + \mathbf{F}(t) = \mathbf{v} \tag{17}$$

in which

$$\mathbf{F}(t) = \mathbf{RI_a} + \mathbf{L}\dot{\mathbf{I}}_{\mathbf{a}} + (\mathbf{K_b}\mathbf{r}^{-1} - \mathbf{I_n})\dot{\mathbf{q}} \tag{18}$$

https://doi.org/10.1017/S026357471500051X Published online by Cambridge University Press

is the lumped uncertainty and $\mathbf{I}_n$ is the identity $n \times n$ matrix. Suppose that $f_i(t)$ is the i^{th} component of $F(t)$. According to the previous section, $f_i(t)$ can be expanded by a Fourier series as

$$f_i(t) = P_i^{*T} \xi_i(t) + \varepsilon_i(t) \tag{19}$$

where $\xi_i(t)$ is of the form (8) and P_i^* is of the form (7). As a result, the vector $\mathbf{F}(t)$ can be represented by

$$\mathbf{F}(t) = \xi \mathbf{P}^* + \boldsymbol{\varepsilon} \tag{20}$$

in which

$$\xi = \text{diag}\left[\xi_1^T(t), \quad \ldots, \quad \xi_n^T(t)\right] \tag{21}$$

$$\mathbf{P}^* = \left[P_1^{*T}, \quad \ldots, \quad P_n^{*T}\right]^T \tag{22}$$

$$\boldsymbol{\varepsilon} = [\boldsymbol{\varepsilon}_1(t), \quad \ldots, \quad \boldsymbol{\varepsilon}_n(t)]^T \tag{23}$$

The control law is proposed as

$$\boldsymbol{v} = \dot{\mathbf{q}}_\mathbf{d} + \mathbf{K}_\mathbf{p}\tilde{\mathbf{q}} + \hat{\mathbf{F}}(t) \tag{24}$$

where $\tilde{\mathbf{q}} = \mathbf{q}_\mathbf{d} - \mathbf{q}$ is the tracking error, $\mathbf{q}_\mathbf{d}$ is the desired trajectory, $\mathbf{K}_\mathbf{p}$ is a diagonal matrix of proportional gain and $\hat{\mathbf{F}}(t)$ is the Fourier series estimation of the lumped uncertainty using m frequencies. Let $\hat{f}_i(t)$ denote the ith component of $\hat{\mathbf{F}}(t)$. According to (6), $\hat{f}_i(t)$ can be given by

$$\hat{f}_i(t) = \hat{P}_i^T \xi_i(t) \tag{25}$$

Consequently, $\hat{\mathbf{F}}(t)$ can be expressed as

$$\hat{\mathbf{F}}(t) = \xi \hat{\mathbf{P}} \tag{26}$$

where $\hat{P} = [\hat{P}_1^T \quad \ldots \quad \hat{P}_n^T]^T$. Assume that $f_i^* = P_i^{*T} \xi_i(t)$ is the best approximation of $f_i(t)$ using m frequencies. Therefore, we have $f_i(t) = P_i^{*T} \xi_i(t) + \boldsymbol{\varepsilon}_i(t)$. Since $f_i(t)$ is uncertain, P_i^* is unknown and its estimation $\hat{P}_i$ is used. The adaptation laws try to make $\hat{P}_i$ converge to P_i^*. Because of the truncation error, even in the ideal case that $\hat{P}_i = P_i^*$ we cannot expect the equality $f_i(t) = \hat{f}_i(t)$. Thus, the control law (24) is modified as

$$v = \dot{\mathbf{q}}_d + \mathbf{K}_\mathbf{p}\tilde{\mathbf{q}} + \hat{\mathbf{F}}(t) + \mathbf{F}_r(t) \tag{27}$$

The robustifying control term $\mathbf{F}_r(t)$ is added to control law with the aim of compensating the truncation error. Using (17) and (27), the closed loop system is given by

$$\mathbf{q}_\mathbf{d} + \mathbf{K}_\mathbf{p}\tilde{\mathbf{q}} + \hat{\mathbf{F}}(t) + \mathbf{F}_\mathbf{r}(t) = \dot{\mathbf{q}} + \mathbf{F}(t) \tag{28}$$

Using (20) and (26), (28) can be simplified as

$$\dot{\tilde{\mathbf{q}}} + \mathbf{K}_\mathbf{p}\tilde{\mathbf{q}} = \xi\tilde{\mathbf{P}} + \boldsymbol{\varepsilon} - \mathbf{F}_\mathbf{r} \tag{29}$$

where $\tilde{P} = P^* - \hat{P}$.

Remark 2 It is worthy of mention that although the control (27) is proposed based on the motor voltage equation only, the manipulator dynamic (9) has not been neglected, since it has been included in the lumped uncertainty $\mathbf{F}(t)$ and compensated in the control law (27). In fact, the motor current I_a is the representative of manipulator dynamic (9) in the motor voltage equation. This can be understood more clearly by considering the relations between (9), (10) and (13) as

$$\mathbf{J}_\mathbf{m}\mathbf{r}^{-1}\ddot{\mathbf{q}} + \mathbf{B}_\mathbf{m}\mathbf{r}^{-1}\dot{\mathbf{q}} + \mathbf{r}\left(\mathbf{D}(\mathbf{q})\ddot{\mathbf{q}} + \mathbf{C}(\mathbf{q}, \dot{\mathbf{q}})\dot{\mathbf{q}} + \mathbf{G}(\mathbf{q})\right) = \mathbf{k}_\mathbf{m}\mathbf{I}_\mathbf{a} \tag{30}$$

https://doi.org/10.1017/S026357471500051X Published online by Cambridge University Press

which implies that the motor currents I_a contains all the nonlinear effects of the manipulator dynamics (9).

5. Stability Analysis

A proof for the bounded-ness of state variables $\mathbf{x}$ in (15) is given by stability analysis and the adaptation laws for the Fourier series coefficients are designed. In order to analyze the stability, the following assumptions are made.

Assumption 1 The desired trajectory $\mathbf{q_d}$ is smooth in the sense that $\mathbf{q_d}$ and its derivatives up to a necessary order are available and all uniformly bounded.[26]

Assumption 2 The truncation error vector is bounded[25] as $\|\boldsymbol{\varepsilon}\| \leq E$ where E is a known constant.

Theorem 1 Consider the dynamical system (17) and the control law (27). The state variable $\mathbf{x}$ is bounded and the tracking error $\tilde{\mathbf{q}}$ asymptotically converges to zero if the following adaptation law holds.

$$\dot{\hat{\mathbf{P}}} = \gamma \tilde{\mathbf{q}} \xi(t) \tag{31}$$

In (31), the $n \times n$ diagonal positive matrix of $\boldsymbol{\gamma}$ determines the convergence rate.

Proof: Consider the following positive definite function.

$$V(t) = \frac{\tilde{\mathbf{q}}^T \tilde{\mathbf{q}}}{2} + \frac{\tilde{\mathbf{P}}^T \tilde{\mathbf{P}}}{2\boldsymbol{\gamma}} \tag{32}$$

The time derivative of (32) given by

$$\dot{V}(t) = \tilde{\mathbf{q}}^T \dot{\tilde{\mathbf{q}}} - \frac{\tilde{\mathbf{P}}^T \dot{\hat{\mathbf{P}}}}{\boldsymbol{\gamma}} \tag{33}$$

Substituting $\dot{\tilde{\mathbf{q}}}$ from (29) into (33) yields

$$\dot{V} = \tilde{\mathbf{q}}^T \left(-\mathbf{K_p} \tilde{\mathbf{q}} + \xi \tilde{\mathbf{P}} + \boldsymbol{\varepsilon} - \mathbf{F_r} \right) - \frac{\tilde{\mathbf{P}}^T \dot{\hat{\mathbf{P}}}}{\boldsymbol{\gamma}} \tag{34}$$

Using (31), we can simplify (34) as

$$\dot{V} = \tilde{\mathbf{q}}^T \left(-\mathbf{K_p} \tilde{\mathbf{q}} + \boldsymbol{\varepsilon} - \mathbf{F_r} \right) \tag{35}$$

It follows from (35) and **Assumption 3** that

$$\dot{V} \leq -\tilde{\mathbf{q}}^T \mathbf{K_p} \tilde{\mathbf{q}} + \left\| \tilde{\mathbf{q}}^T E \right\| - \tilde{\mathbf{q}}^T \mathbf{F_r} \tag{36}$$

According to Qu *et al.*,[1] we can propose the robustifying control term $\mathbf{F_r}$ as

$$\mathbf{F_r} = \frac{\mathbf{y} E}{\|\mathbf{y}\| + \lambda e^{-\delta t}} \tag{37}$$

in which λ and δ are positive scalars and $y = E\tilde{\mathbf{q}}$. Substituting (37) into (36) and some simple manipulations yields

$$\dot{V} \leq -\tilde{\mathbf{q}}^T \mathbf{K_p} \tilde{\mathbf{q}} + \frac{\left\| \tilde{\mathbf{q}}^T E \right\| \lambda e^{-\delta t}}{\|y\| + \lambda e^{-\delta t}} \tag{38}$$

https://doi.org/10.1017/S026357471500051X Published online by Cambridge University Press

Using the inequality $\frac{ab}{a+b} < a \quad \forall a, b > 0$, (38) can be rewritten as

$$\dot{V} \leq -\tilde{\mathbf{q}}^T \mathbf{K_p} \tilde{\mathbf{q}} + \lambda e^{-\delta t} \tag{39}$$

According to Qu *et al.*,[1] (39) implies that $\tilde{\mathbf{q}}$ asymptotically converges to zero and $\tilde{\mathbf{P}}$ is bounded. Consequently, F_r and $\hat{F}$ are bounded. Using **Assumption 1**, bounded-ness of the control law (27) is obtained. Since motor voltages are bounded, $\dot{\mathbf{q}}$ and $\mathbf{I_a}$ are bounded.[20] Thus, the state vector $\mathbf{x}$ is bounded.

6. Fundamental Period of Fourier Series

In this section, the proper value of fundamental period duration of Fourier series is discussed. Suppose that $q_{di}(t)$ is the ith component of the desired trajectory $\mathbf{q_d}(t)$ and $q_{di}(t)$ is a periodic function with fundamental period duration T_{di}. Since it is assumed that the lumped uncertainty $\mathbf{F}(t)$ is not available, its frequency content cannot be determined precisely. Therefore, we cannot state this paper's finding as a general theorem and present an exact proof. However, in this section, it is intuitively shown that if LCM(T_{d1}, ..., T_{dn}) is chosen as the fundamental period duration of the Fourier series expansion (26), and then we can include frequency contents of $\mathbf{F}(t)$ in the vector $\xi(t)$ in (21) as much as possible. First, consider the following preliminaries.

For positive rational numbers a and b, define $[a, b]$ as the least common multiple of a and b. Also, define the greatest common devisor (GCD) of a and b as (a, b). According to Hardy *et al.*,[27] given two rational numbers $a = \prod_i p_i^{n_i}$ and $b = \prod_i p_i^{m_i}$ where the exponents n_i and m_i are the integer numbers and p_i is the prime number, their GCD and LCM are calculated by the formulas

$$(a, b) = \prod_i p_i^{\min(n_i, m_i)} \tag{40}$$

$$[a, b] = \prod_i p_i^{\max(n_i, m_i)} \tag{41}$$

Also, we have the following properties:[27]

$$[a, b] \times (a, b) = ab \tag{42}$$

$$[ca, cb] = c[a, b] \tag{43}$$

$$(a, b) = (a + b, b) \tag{44}$$

$$\left[\frac{1}{a}, \frac{1}{b}\right] = \frac{1}{(a, b)} \tag{45}$$

where c is a positive rational number. In order to prove (45), we can write

$$\left[\frac{1}{a}, \frac{1}{b}\right] = \left[\frac{b}{ab}, \frac{a}{ab}\right] = \frac{[a, b]}{ab} = \frac{1}{(a, b)} \tag{46}$$

Lemma 1: $(2a, b) = \begin{cases} (a, b) \\ 2(a, b) \end{cases}$.

Proof: please refer to **Appendix 1**.

Lemma 2: The fundamental period duration of $y(t) = \cos(\omega_1 t + \alpha_1) \pm \sin(\omega_2 t + \alpha_2)$ is given by $[T_1, T_2]$ in which $T_1 = 2\pi / \omega_1$ and $T_2 = 2\pi / \omega_2$.

https://doi.org/10.1017/S026357471500051X Published online by Cambridge University Press

Proof: please refer to **Appendix 2**.

Examples: Suppose that in **Lemma 2**, we have $T_1 = 12$ and $T_2 = 30$. Thus, $[T_1, T_2]$ is given by

$$[2^2 \times 3^1 \times 5^0, 2^1 \times 3^1 \times 5^1] = 2^{\max(2,1)} \times 3^{\max(1,1)} \times 5^{\max(0,1)} = 60 \tag{47}$$

Consider a more general case in which $T_1 = 1/3$ and $T_2 = 1/4$. Thus, $[T_1, T_2]$ is calculated as

$$[3^{-1} \times 2^0, 3^0 \times 2^{-2}] = 3^{\max(-1,0)} \times 2^{\max(0,-2)} = 1 \tag{48}$$

For another example, $[\frac{\pi}{3}, \frac{2\pi}{5}]$ is given by

$$[2^0 \times 3^{-1} \times 5^0 \times \pi^1, 2^1 \times 3^0 \times 5^{-1} \times \pi^1] = 2^{\max(0,1)} \times 3^{\max(-1,0)} \times 5^{\max(0,-1)} \times \pi^1 = 2\pi \tag{49}$$

Lemma 3: Suppose that T_1 and T_2 belong to positive rational numbers. The fundamental period duration of functions such as

$$x(t) = \cos\left(\frac{2\pi}{T_1}t + \alpha_1\right) \times \sin\left(\frac{2\pi}{T_2}t + \alpha_2\right) \tag{50}$$

is given by

$$T_1 T_2 \left[\frac{1}{|T_1 - T_2|}, \frac{1}{T_1 + T_2}\right] = \frac{[T_1, T_2]}{K} \tag{51}$$

in which $K = 1$ or $K = 2$.

Proof: Please refer to **Appendix 3**.

Remark 3: In the case that T_1 and T_2 belong to irrational numbers, $x(t)$ and $y(t)$ are not generally periodic. Nevertheless, we can approximate T_1 and T_2 by rational numbers. Thus, we can approximate $x(t)$ and $y(t)$ by sinusoidal periodic functions. This issue has been investigated with more details in **Simulation 3**.

Lemma 4: Suppose that there are j sinusoidal functions in $x(t)$ defined by (50) such that $j \geq 3$. Then, the fundamental period duration of $x(t)$ is given by $[T_1, T_2, \cdots, T_j]/K$ in which $K \in \left\{1, 2, 4, \cdots, 2^{j-1}\right\}$.

Proof: Please refer to **Appendix 4**.

Now, we can focus on the lumped uncertainty $\mathbf{F}(t)$. According to (30), we have

$$\mathbf{I_a} = \mathbf{K_m^{-1}}\left(\mathbf{J_m r^{-1}\ddot{q}} + \mathbf{B_m r^{-1}\dot{q}} + \mathbf{r}\left(\mathbf{D\ddot{q}} + \mathbf{C\dot{q}} + \mathbf{G}\right)\right) \tag{52}$$

Using (52) and its time derivative, the lumped uncertainty $\mathbf{F}(t)$ in (18) can be rewritten as

$$\mathbf{F}(t) = \mathbf{F}_1(\mathbf{q})\ddot{\mathbf{q}} + \mathbf{F}_2(\mathbf{q}, \dot{\mathbf{q}})\ddot{\mathbf{q}} + \mathbf{F}_3(\mathbf{q}, \dot{\mathbf{q}})\dot{\mathbf{q}} + \mathbf{F}_4(\mathbf{q}, \dot{\mathbf{q}}) \tag{53}$$

where $\mathbf{F}_1(\mathbf{q}) = \mathbf{LK_m^{-1}rD(q)}$ and

$$\mathbf{F}_2(\mathbf{q}, \dot{\mathbf{q}}) = \mathbf{RK_m^{-1}}\left(\mathbf{J_m r^{-1}} + \mathbf{rD}\right) + \mathbf{LK_m^{-1}}\left(\mathbf{B_m r^{-1}} + \mathbf{r\dot{D}} + \mathbf{rC}\right) + \mathbf{K_b r^{-1}} - \mathbf{I_n} \tag{54}$$

$$\mathbf{F}_3(\mathbf{q}, \dot{\mathbf{q}}) = \mathbf{RK_m^{-1}}\left(\mathbf{B_m r^{-1}} + \mathbf{rC(q, \dot{q})}\right) + \mathbf{LK_m^{-1}r\dot{C}(q, \dot{q})} \tag{55}$$

$$\mathbf{F}_4(\mathbf{q}, \dot{\mathbf{q}}) = \mathbf{RK_m^{-1}rG(q)} + \mathbf{LK_m^{-1}r\dot{G}(q, \dot{q})} \tag{56}$$

https://doi.org/10.1017/S026357471500051X Published online by Cambridge University Press

According to the stability analysis, in the sinusoidal steady state, the joint position $\mathbf{q}$ and its time derivatives converge to their desired trajectories. Thus, in the sinusoidal steady state, $\mathbf{F}(t)$ can be given by

$$\mathbf{F}_{ss}(t) = \mathbf{F}_1(\mathbf{q_d})_\mathbf{d} + \mathbf{F}_2(\mathbf{q_d}, \dot{\mathbf{q}}_\mathbf{d})\ddot{\mathbf{q}}_\mathbf{d} + \mathbf{F}_3(\mathbf{q_d}, \dot{\mathbf{q}}_\mathbf{d})\dot{\mathbf{q}}_\mathbf{d} + \mathbf{F}_4(\mathbf{q_d}, \dot{\mathbf{q}}_\mathbf{d}) \tag{57}$$

According to Spong *et al.*,[26] the homogenous transformation matrix $T_0^n(q)$ that expresses the coordinate frame attached to nth link with respect to the base coordinate frame is of the form

$$T_0^n(q) = \begin{bmatrix} R_0^n(q) & d_0^n(q) \\ 0 & 1 \end{bmatrix} = A_1 A_2 ... A_n \tag{58}$$

in which R_0^n and d_0^n are the orientation and position of nth coordinate frame with respect to the base coordinate frame and A_i is given by

$$\begin{aligned} A_i &= \mathrm{Rot}_{Z,\theta_i} \times \mathrm{Trans}_{Z,d_i} \times \mathrm{Trans}_{X,a_i} \times \mathrm{Rot}_{X,\alpha_i} \\ &= \begin{bmatrix} C_{\theta_i} & -S_{\theta_i} C_{\alpha_i} & S_{\theta_i} S_{\alpha_i} & a_i C_{\theta_i} \\ S_{\theta_i} & C_{\theta_i} C_{\alpha_i} & -C_{\theta_i} S_{\alpha_i} & a_i S_{\theta_i} \\ 0 & S_{\alpha_i} & C_{\alpha_i} & d_i \\ 0 & 0 & 0 & 1 \end{bmatrix} \end{aligned} \tag{59}$$

The four quantities θ_i, a_i, d_i, and α_i are link length, link twist, link off-set, and joint angle, respectively. Also, $C_\theta = \cos(\theta)$ and $S_\theta = \sin(\theta)$. Therefore, R_0^n and d_0^n are composed of some sinusoidal and constant elements.

The manipulator Jacobian matrix $\mathbf{J}_0^n \in R^{6\times n}$ relates joints-space velocities $\dot{\mathbf{q}}$ to task-space velocities $\dot{\mathbf{X}}$ as

$$\dot{\mathbf{X}} = \mathbf{J}_0^n \dot{\mathbf{q}} \tag{60}$$

Suppose that $\mathbf{J}_i$ is the ith column of $\mathbf{J}_0^n$. For a prismatic joint, we have

$$\mathbf{J}_i = \mathbf{J}_{\mathbf{v}_i} = \begin{bmatrix} \mathbf{Z}_{i-1} \\ \mathbf{0} \end{bmatrix} \tag{61}$$

in which $\mathbf{Z}_i$ is given by the first three components in the third column of T_0^i. Also, for each revolute joint, $\mathbf{J}_i$ is given by

$$\mathbf{J}_i = \mathbf{J}_{\boldsymbol{\omega}_i} = \begin{bmatrix} \mathbf{Z}_{i-1} \times (\mathbf{O}_n - \mathbf{O}_{i-1}) \\ \mathbf{Z}_{i-1} \end{bmatrix} \tag{62}$$

where $\mathbf{O}_n$ is given by the first three components in the fourth column of T_0^n. Thus, $\mathbf{J}_{\mathbf{v}_i}$ and $\mathbf{J}_{\boldsymbol{\omega}_i}$ are composed of some sinusoidal and constant terms, respectively.

The manipulator inertia matrix $\mathbf{D}(\mathbf{q})$ is calculated as

$$\mathbf{D}(\mathbf{q}) = \sum_{i=1}^{n} \left[m_i \mathbf{J}_{\mathbf{v}_i}^T \mathbf{J}_{\mathbf{v}_i} + \mathbf{J}_{\boldsymbol{\omega}_i}^T \mathbf{R}_i \mathbf{I}_i \mathbf{R}_i^T \mathbf{J}_{\boldsymbol{\omega}_i} \right] \tag{63}$$

in which m_i is the mass of ith link, $\mathbf{R}_i$ is the orientation of ith coordinate frame with respect to the base coordinate frame, and $\mathbf{I}_i$ is the inertia tensor. One can easily obtain from (58)–(63) that $\mathbf{D}(\mathbf{q})$ consists of some sinusoidal and constant components. According to the stability analysis in the previous section, in the sinusoidal steady state, the joint variables q_i $i = 1, \cdots, n$ converge to their desired trajectories. Thus, in the sinusoidal steady state, $\mathbf{D}(\mathbf{q})$ converges to $\mathbf{D}(\mathbf{q}_d)$. The sinusoidal components of $\mathbf{D}(\mathbf{q}_d)$ are combinations of some summations and products of sinusoidal terms with the fundamental period durations T_{d1}, T_{d2},..., and T_{dn}. Therefore, using **Lemma 2**, **Lemma 3** and **Lemma 4**, we can intuitively conclude that the fundamental period duration of each

https://doi.org/10.1017/S026357471500051X Published online by Cambridge University Press

element in $\mathbf{D}(\mathbf{q}_d)$and $\mathbf{F}_1(\mathbf{q_d})$ may be given by $[T_{d1}, ..., T_{dn}]/K$ where $K \in \{1, 2, 4, \cdots, 2^{j-1}\}$. For example, suppose that the fundamental period duration of an element in $\mathbf{D}(\mathbf{q}_d)$ is $[T_{d1}, ..., T_{dn}]/K$ which corresponds to $\omega = 2K\pi / [T_{d1}, ..., T_{dn}]$. Thus, it is obvious that if we choose $[T_{d1}, ..., T_{dn}]$ as the fundamental period duration of Fourier series expansion, other possible harmonics such as $\omega = 2K\pi / [T_{d1}, ..., T_{dn}]$ will be included in the Fourier series expansion.

The potential energy of link i is given by[26]

$$PE_i = g^T r_{ci} m_i \tag{64}$$

where g is the vector giving the direction of gravity in the inertial frame and the vector r_{ci} gives the coordinates of the center of mass of link i. The potential energy for an n-link robot is given by

$$PE = \sum_{i=1}^{n} PE_i \tag{65}$$

Generally, PE is a function of joint variables q_1, q_2,...,q_n. Therefore, using **Lemma 2**, **Lemma 3** and **Lemma 4**, we can state that $[T_{d1}, ..., T_{dn}]$ will be an acceptable selection for the fundamental period duration of potential energy Fourier series expansion.

According to Spong *et al.*,[26] Eq. (9) can be written as

$$\sum_i d_{kj}(\mathbf{q})\ddot{q}_j \; + \; \sum_{i,j} c_{ijk}(\mathbf{q})\dot{q}_i\dot{q}_j \; + \; \varphi_k(\mathbf{q}) = \tau_k \quad k = 1, ..., n \tag{66}$$

where $c_{ijk} = \frac{1}{2}\{\frac{\partial d_{kj}}{\partial q_i} + \frac{\partial d_{ki}}{\partial q_j} - \frac{\partial d_{ij}}{\partial q_k}\}$ and $\varphi_k(\mathbf{q}) = \frac{\partial PE}{\partial q_k}$. Potential energy and all elements of the inertia matrix are the sinusoidal function of q_i $i = 1, ..., n$. Therefore, differentiating them with respect to q_i will not change the fundamental period duration. Thus, $[T_{d1}, ..., T_{dn}]$ is a proper value for the fundamental period durations of functions c_{ijk}, φ_k, $\mathbf{C}(\mathbf{q_d}, \dot{\mathbf{q}}_\mathbf{d})\dot{\mathbf{q}}_\mathbf{d}$, $\mathbf{G}(\mathbf{q_d})$, $\mathbf{F}_1(\mathbf{q_d})\ddot{\mathbf{q}}_\mathbf{d}$, $\mathbf{F}_2(\mathbf{q_d}, \dot{\mathbf{q}}_\mathbf{d})\ddot{\mathbf{q}}_\mathbf{d}$, $\mathbf{F}_3(\mathbf{q_d}, \dot{\mathbf{q}}_\mathbf{d})\dot{\mathbf{q}}_\mathbf{d}$, $\mathbf{F}_4(\mathbf{q_d}, \dot{\mathbf{q}}_\mathbf{d})$. Consequently, the same result is obtained for $\mathbf{F}_{ss}(t)$ in (57).

This section can be summarized as the following remark.

Remark 4 Consider the problem of robust tracking control of electrically driven robot manipulators described by (14) and the control law (27). In order to estimate the lumped uncertainty $\mathbf{F}(t)$ using Fourier series, $[T_{d1}, ..., T_{dn}]$ can be a good choice for the fundamental period duration of $\xi_i(t)$ in the Fourier series expansion (26). Thus, the vector $\xi_i(t)$ can be arranged as

$$\xi_i(t) = \begin{bmatrix} 1 & \cos\omega_0 t & \sin\omega_0 t & \cos 2\omega_0 t & \sin 2\omega_0 t & \cdots & \cos m\omega_0 t & \sin m\omega_0 t \end{bmatrix}^T \tag{67}$$

where $\omega_0 = 2\pi/[T_{d1}, ..., T_{dn}]$.

7. Simulation Results

In this section, the performance of proposed control law (27) is evaluated. The case study is a SCARA manipulator actuated by permanent magnet DC motors. The Denavit–Hartenberg (DH) parameters, manipulator dynamic parameters, and motor parameters are given in Tables I, II and III, respectively. In the simulations, the arm which consists of the first three joints is used to perform the proposed task-space control law and the fourth joint is locked.[28] Simulation 1 deals with the estimation effects of Fourier series. Also, to verify the effectiveness of applying Fourier series for uncertainty estimation, different periodic trajectories are defined. In Simulation 2, the effects of different selections for the fundamental period duration of Fourier series are studied. In Simulation 3, it has been assumed that the fundamental period durations of desired trajectories are irrational numbers. Simulation 4 deals with non-periodic motions and Simulation 5 examines the proposed method in a higher frequency. Simulation 6 deals with the noise problem. In order to compare the performance of the proposed controller with previous related works, a voltage-based controller using neuro-fuzzy systems has been selected.[29] In Simulation 6, this comparison has been presented.

https://doi.org/10.1017/S026357471500051X Published online by Cambridge University Press

Table I. The Denavit−Hartenberg parameters.

link	θ(rad)	$d(m)$	$a(m)$	α(rad)
1	θ_1	0	$a_1 = 0.621$	0
2	θ_2	0	$a_2 = 1.064$	π
3	0	d_3	0	0
4	θ_4	$d_4 = 0.05$	0	0

Table II. The dynamical parameters.

I_{yzi}	I_{xzi}	I_{xyi}	I_{zzi}	I_{yyi}	I_{xxi}	m_i	z_i	y_i	x_i	link
0.0001	−0.002	0.02	7.6	7.31	1.62	95.23	−0.14	−0.001	−0.308	1
−0.001	2.1	0.0135	21.68	22.64	3.74	158.09	−0.19	0.001	−0.674	2
0	−0.0004	0	0.04	1.63	1.63	16.62	−0.54	0	0	3
0	0	0	0	0	0	0.106	−0.025	0	0	4

Table III. Motor parameters.

Motor	R	$k_m = k_b$	J_m	B_m	r	L
1, 2, 3	1	0.36	0.0002	0.001	0.008	0.001

7.1. Simulation 1: the proposed fundamental period duration

Suppose that the desired trajectories are defined as

$$\mathbf{q_d} = \begin{bmatrix} 1 - \cos(2\pi t/3) \\ 1 - \cos(2\pi t/2) \\ 1 - \cos(2\pi t/4) \end{bmatrix} \tag{68}$$

which implies that $T_{d1} = 3$, $T_{d2} = 2$ and $T_{d3} = 4$. It is obvious that for the SCARA manipulator illustrated in Fig. 1, the kinetic and potential energy of the third link are independent from θ_1 and θ_2. In other words, there are some couplings between the first two links, while the third link is quite decoupled from the first two links. Thus, we can choose $T = [T_{d1}, T_{d2}]$ and T_{d3} as the fundamental period duration of Fourier series for the first two elements of $\mathbf{F}(t)$ and the third elements of $\mathbf{F}(t)$, respectively. As a result, the matrix ξ in (21) can be of the form

$$\boldsymbol{\xi}(t) = \text{diag}(\xi_1^T, \xi_2^T, \xi_3^T) \tag{69}$$

$$\xi_1 = \xi_2 = \begin{bmatrix} 1 & \cos\omega t & \sin\omega t & \cdots & \cos m\omega t & \sin m\omega t \end{bmatrix}^T \tag{70}$$

$$\xi_3 = \begin{bmatrix} 1 & \cos\omega_3 t & \sin\omega_3 t & \cdots & \cos m\omega_3 t & \sin m\omega_3 t \end{bmatrix}^T \tag{71}$$

where $\omega = 2\pi/T = 2\pi/6$ and $\omega_3 = 2\pi/T_{d3} = 2\pi/4$. Suppose that $m = 6$ is selected. The initial values of all Fourier series coefficients $\hat{\mathbf{P}}(0)$ are set to zero. The learning rate γ is set 10,000 to make $\hat{\mathbf{P}}(t)$ converge to its actual value as fast as possible. The proportional gain $\mathbf{K_p}$ is set to $\mathbf{K_p} = 25000\mathbf{I}_3$ to make the tracking error as small as possible. The parameters E, λ and δ in (37) are set to 1. In order to have better comparisons, the following cost function is defined.

$$C_f = \int_0^{25} \|\tilde{\mathbf{q}}(t)\| dt \tag{72}$$

The tracking errors and convergence of Fourier series coefficients for the first joint have been illustrated in Figs. 1 and 2, respectively. As shown is Fig. 1, the tracking errors converge to zero

https://doi.org/10.1017/S026357471500051X Published online by Cambridge University Press

Table IV. The effect of increasing m in Simulation 1.

m	4	6	8	10	12
C_f	0.0289	0.0265	0.0259	0.0257	0.0256

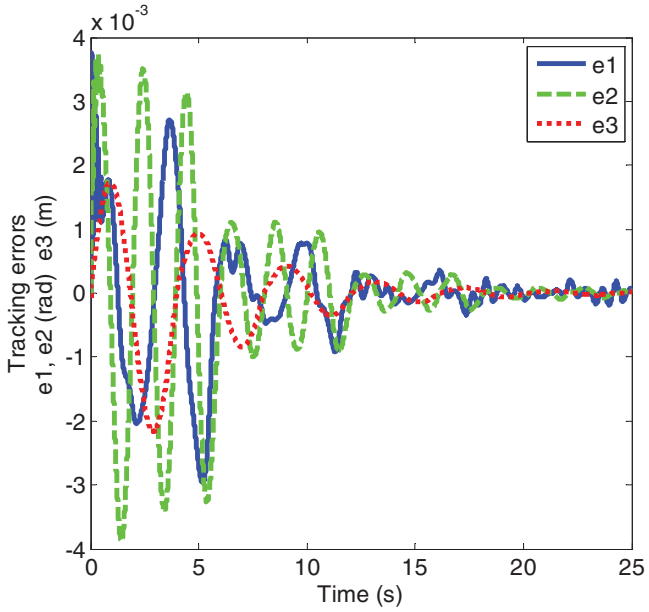


Fig. 1. The tracking errors in Simulation 1.

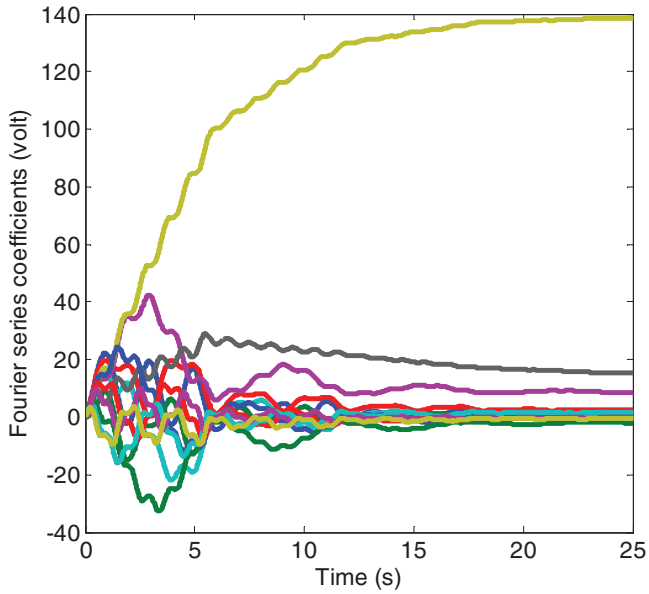


Fig. 2. The convergence of Fourier series coefficients for the first joint in Simulation 1.

asymptotically. The tracking errors have reduced considerably after 16 sec. According to Fig. 2, this is the time after that the Fourier series coefficients have converged to constant values. In order to evaluate the effect of increasing the number of frequencies in Fourier series expansion, we have increased m to 8, 10 and 12. Table IV shows the results. According to this table, it seems that six frequencies are sufficient and there is no need to increase them. The control efforts are illustrated in Fig. 3. As shown in this figure, motor voltages are smooth without any chattering.

https://doi.org/10.1017/S026357471500051X Published online by Cambridge University Press

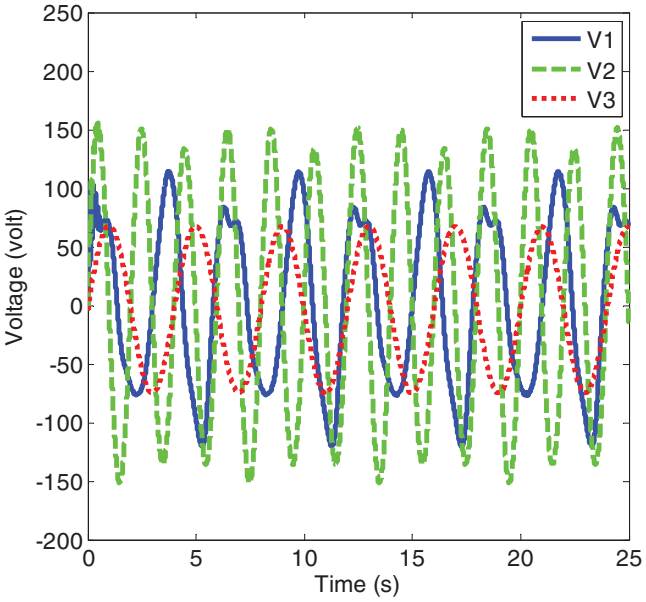


Fig. 3. The control efforts in Simulation 1.

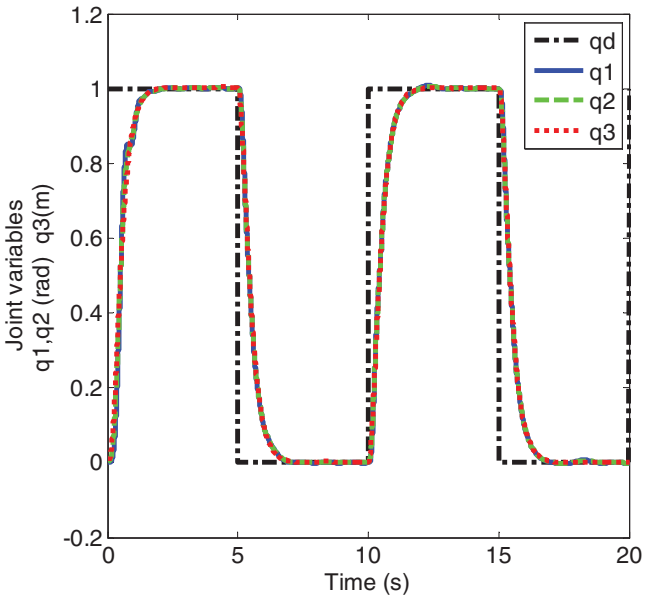


Fig. 4. The performance of proposed method in tracking a square wave trajectory.

Finding the optimum value of m is not our goal. In fact, the use of optimum value of m is not effective since the truncation error is compensated. The simulation was repeated many times to find out many terms are not needed for Fourier series. Our aim is to show that although increasing m reduces the tracking error, its effect is ignorable.

Figure 4 shows the performance of the proposed method in tracking a square wave trajectory and Fig. 5 represents the motor voltages. The transfer function $G(s) = \frac{16}{s^2+8s+16}$ has been used as a reference model to control the transient response. Also, a triangle wave trajectory has been defined as the desired trajectory. The tracking performance and motor voltages are illustrated in Figs. 6 and 7, respectively. The smooth control effort with no chattering is advantageous since implementing of this signal is easy and there are no effects of chattering such as vibration. However, in a real-world experiment, motor voltage may not be smooth due to the sensor noise. These figures indicate the proposed controller ability in tracking various periodic trajectories.

https://doi.org/10.1017/S026357471500051X Published online by Cambridge University Press

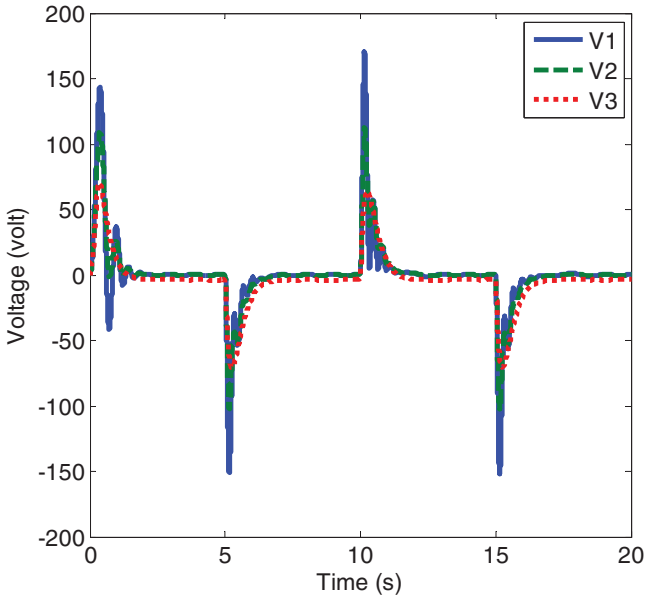


Fig. 5. The control efforts in tracking a square wave trajectory.

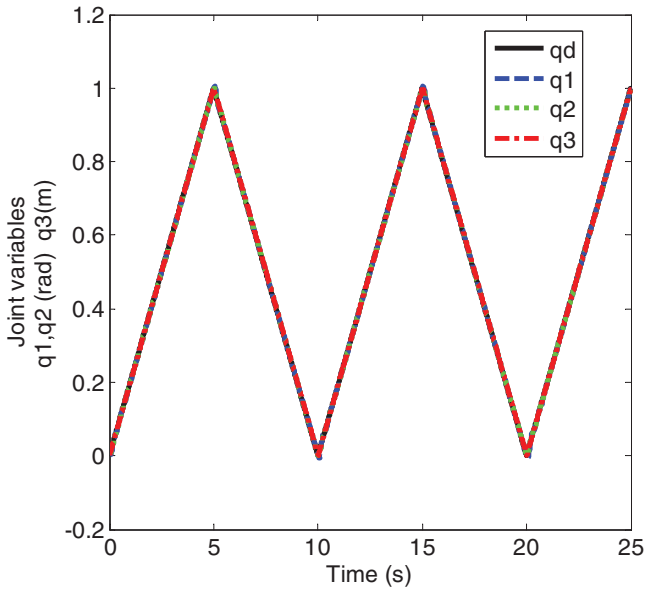


Fig. 6. The performance of proposed method in tracking a triangle wave trajectory.

The Fourier series coefficients they converge to a constant value in about 16 S. However, according to the stability analysis, the tracking error converges to zero regardless of the status of the Fourier series coefficients. The tracking error is satisfactory even before the convergence of the Fourier series coefficients. In fact, the proportional gain $\mathbf{K_p}$ plays the most important role in the satisfactory performance of the controller. Convergence of the Fourier series coefficients just plays a *fine tuning role* around the best response. In order to verify our claims, we have set these coefficients to their final values and also the convergence rate gamma to zero. In this situation, if $\mathbf{K_p}$ is set to $250\mathbf{I}_3$, then $C_f = 0.155$ and if $\mathbf{K_p} = 25000\mathbf{I}_3$, then C_f reduces to 0.002. Therefore, the role of $\mathbf{K_p}$ is more dominant than the role of Fourier series coefficients convergence in the tracking error.

The response of robotic system to some trajectories such as the sinusoid signal, step signal and triangular signal were evaluated to find the proper value to the fundamental period duration of Fourier series. The high control efforts are not provided if the actuators are saturated. According to the

https://doi.org/10.1017/S026357471500051X Published online by Cambridge University Press

Table V. The effects of fundamental period duration and number of used frequencies.

C_f	$m = 4$	$m = 6$	$m = 8$	$m = 10$	$m = 12$
$T = 1.5$	0.1243	0.1243	0.1243	0.1243	0.1243
$T = 2$	0.0842	0.0842	0.0842	0.0842	0.0842
$T = 2.5$	0.1165	0.1166	0.1167	0.1168	0.1169
$T = 5$	0.1136	0.1144	0.1146	0.1148	0.1149
$T = 8$	0.0638	0.0628	0.0627	0.0626	0.0623
$T = 10$	0.0868	0.0649	0.0658	0.0661	0.0665
$T = 12$	0.0761	0.0360	0.0345	0.0332	0.0324
$T = 15$	0.0879	0.0655	0.0585	0.0617	0.0629

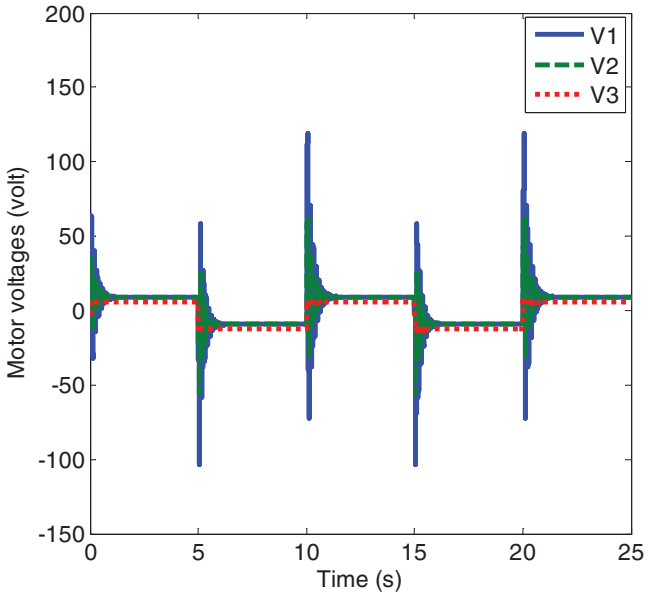


Fig. 7. The control efforts in tracking a triangle wave trajectory.

simulation results in Figs. 3, 5, and 7, the control efforts are under 200 V in response to the used signals. Regarding the template values of motors, using motors with nominal voltages of 200 V is okay. It is assumed that these motors are not saturated under the nominal voltages.

7.2. Simulation 2: other fundamental period durations

In this simulation, the effect of the fundamental period duration is investigated. Table V, shows the values of cost function (72) for different values of fundamental period duration and number of used frequencies. In this simulation, it has been assumed that T is the fundamental period duration for all joints and the desired trajectory is given by (68). All other controller parameters are the same as Simulation 1. Table V indicates that when the fundamental period duration is not set to the best value proposed by this paper, neither increasing the number of used frequencies nor changing the fundamental period duration can reduce the cost function and the tracking error.

7.3. Simulation 3: irrational numbers

In this simulation, we assume that the fundamental period duration of the desired trajectories are irrational numbers. For example, consider the following trajectories.

$$\mathbf{q_d} = \begin{bmatrix} 1 - \cos(2\pi t/\sqrt{10}) \\ 1 - \cos(2\pi t/\sqrt{5}) \\ 1 - \cos(2\pi t/\sqrt{17}) \end{bmatrix} \tag{73}$$

https://doi.org/10.1017/S026357471500051X Published online by Cambridge University Press

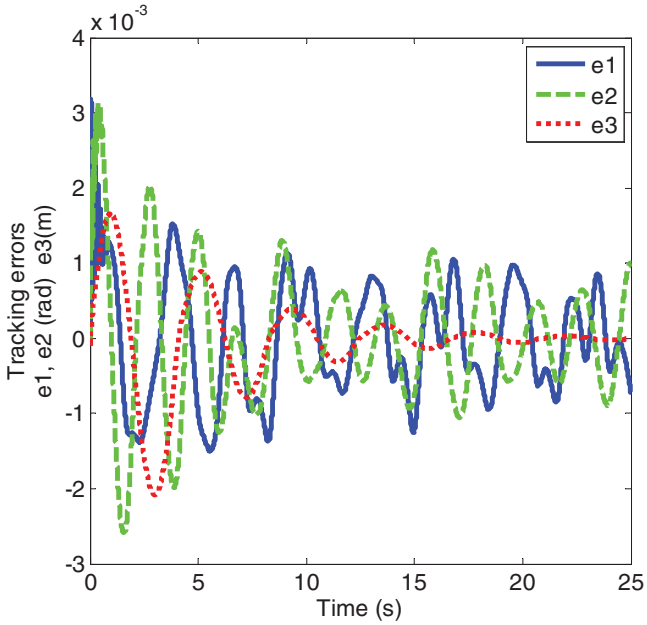


Fig. 8. The tracking errors in Simulation 3.

We can approximate the irrational number $\sqrt{10}$ by the rational number $316/100$. Similarly, we can approximate $\sqrt{5}$ by $223/100$. As a result, the matrix ξ in (23) can be of the form

$$\boldsymbol{\xi}(t) = \text{diag}(\xi_1^T, \xi_2^T, \xi_3^T) \tag{74}$$

$$\xi_1 = \xi_2 = \begin{bmatrix} 1 & \cos\omega t & \sin\omega t & \cdots & \cos m\omega t & \sin m\omega t \end{bmatrix}^T \tag{75}$$

$$\xi_3 = \begin{bmatrix} 1 & \cos\omega_3 t & \sin\omega_3 t & \cdots & \cos m\omega_3 t & \sin m\omega_3 t \end{bmatrix}^T \tag{76}$$

in which $\omega_3 = 2\pi/\sqrt{17}$ and

$$\omega = \frac{2\pi}{lcm(316/100, 223/100)} = \frac{2\pi}{7.0468} \tag{77}$$

The controller parameters values are given in Simulation 1. The tracking errors and control efforts have been illustrated in Figs. 8 and 9, respectively. As shown in Fig. 8, the final values of tracking errors are not greater than 0.001 and the cost function C_f for this simulation is 0.0287. Also, according to Fig. 9, voltages of motors are permitted. These figures confirm that the proposed method has a satisfactory performance in tracking trajectories with irrational fundamental period durations.

Showing advantages of irrational numbers is not our purpose. Since the LCM cannot be defined for irrational numbers, one may conclude that the proposed method does not work for the irrational numbers. Therefore, the mentioned solution was presented in this paper.

7.4. Simulation 4: non-periodic trajectories

The stability analysis is given for a general case. The assumption of periodic trajectories has not been used in the stability analysis. According to stability analysis, if the desired trajectory satisfies the condition stated in Assumption 1, then the tracking error will asymptotically converge to zero. This assumption of periodic functions is required just for Section 6 where the fundamental period duration is determined. To verify the performance of proposed controller for a non-repetitive motion, consider

https://doi.org/10.1017/S026357471500051X Published online by Cambridge University Press

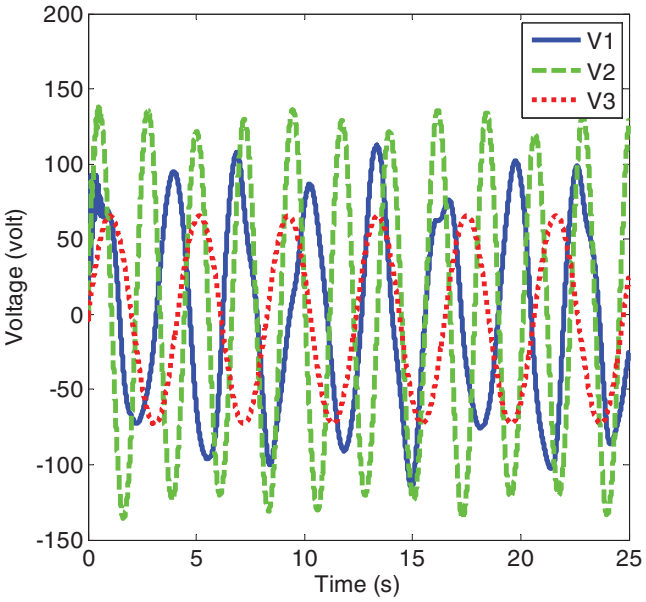


Fig. 9. The control efforts in Simulation 3.

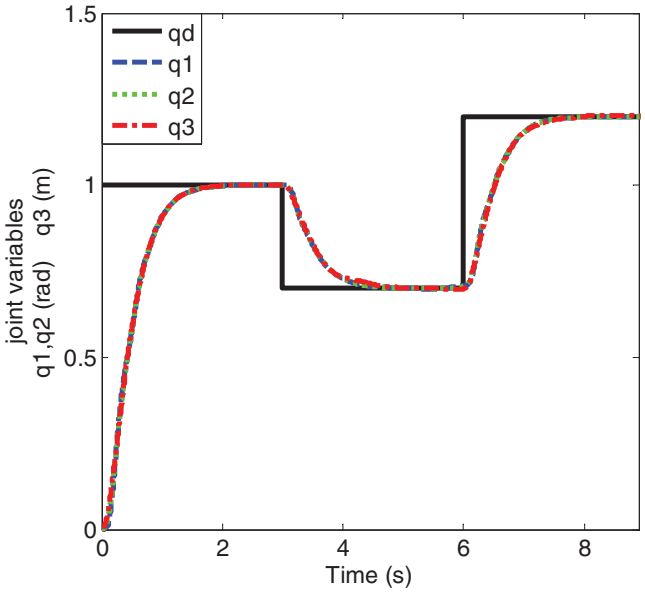


Fig. 10. The tracking performance for a non-periodic motion.

the desired trajectory illustrated in Fig. 10. As shown in this figure, the proposed controller can track non-periodic trajectories very well. Motor voltages for this simulation are presented in Fig. 11.

7.5. Simulation 5: dealing with noise

Suppose that a zero mean Gaussian noise with standard deviation of 0.0002 is added to the position feedbacks. To attenuate the noise problem in sensors, usually low-pass filters are suitable solutions. In this paper, a low-pass filter with the transfer function $G(s) = \frac{1}{0.01s+1}$ is selected to filter the output of the position sensor. Moreover, to prevent from the chattering phenomenon, the proportional gain $\mathbf{K_p}$ and the convergence rate γ have been reduced 10 times. The tracking errors and the control efforts are presented in Figs. 12 and 13, respectively. These figures verify the satisfactory performance of the proposed method in dealing with noisy feedbacks.

https://doi.org/10.1017/S026357471500051X Published online by Cambridge University Press

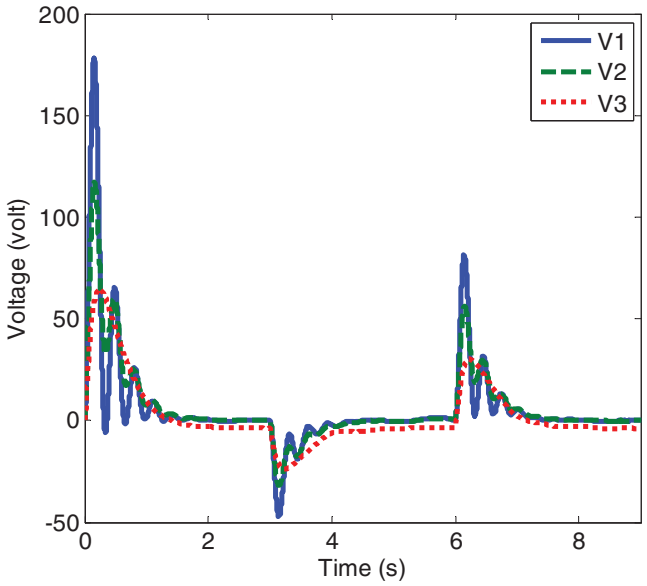


Fig. 11. Motor voltages in a non periodic motion.

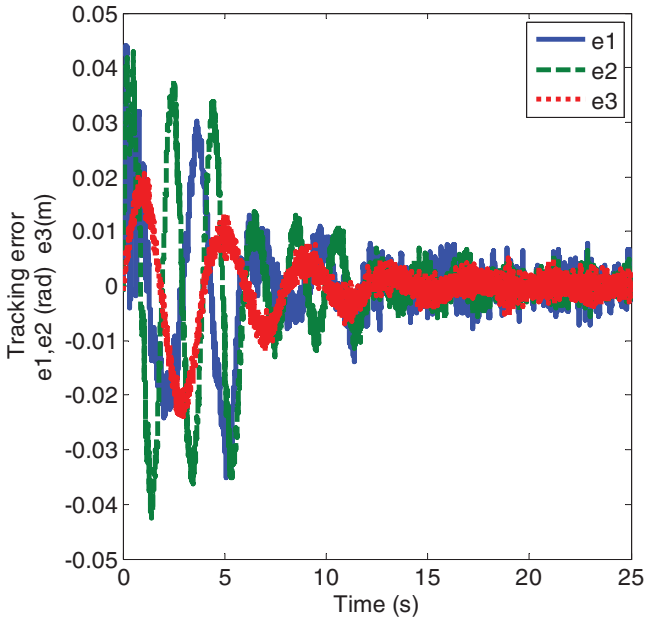


Fig. 12. The tracking errors in Simulation 5.

7.6. Simulation 6: comparison with a neuro-fuzzy controller

A voltage-based controller using adaptive neuro-fuzzy systems has been presented in Wai *et al.*[29] Similar to the proposed method, DC motors are considered as actuators. Feedbacks from joint positions and velocities are required for implementation of the control law in Wai *et al.*,[29] while the proposed controller uses just the position feedback. All of the neuro-fuzzy system parameters such as the mean and standard deviation of the Gaussian membership functions and the weights of output layer are trained using adaptation laws. According to ref. [29], the membership functions are tuned based on the maximum variation of the error function. The parameters K_a and K_b in the error function have been set to $30\mathbf{I}_3$ and $225\mathbf{I}_3$, respectively. Three Gaussian membership functions have been considered for each joint. The initial values of α_i $(0 \leq i \leq 3)$ have been selected randomly in the interval (0, 10) and the initial values of means of Gaussian membership functions have been randomly set to interval$(-12.5, 12.5)$. The standard deviation of all membership functions has been

https://doi.org/10.1017/S026357471500051X Published online by Cambridge University Press

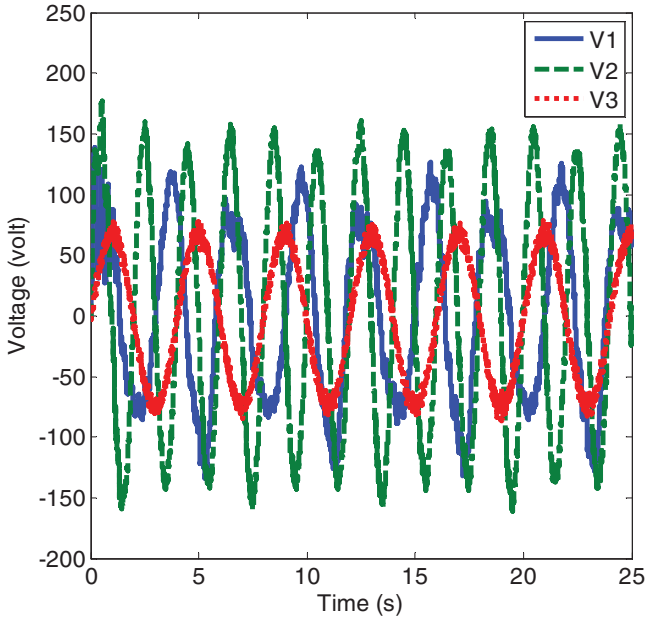


Fig. 13. The control efforts in Simulation 5.

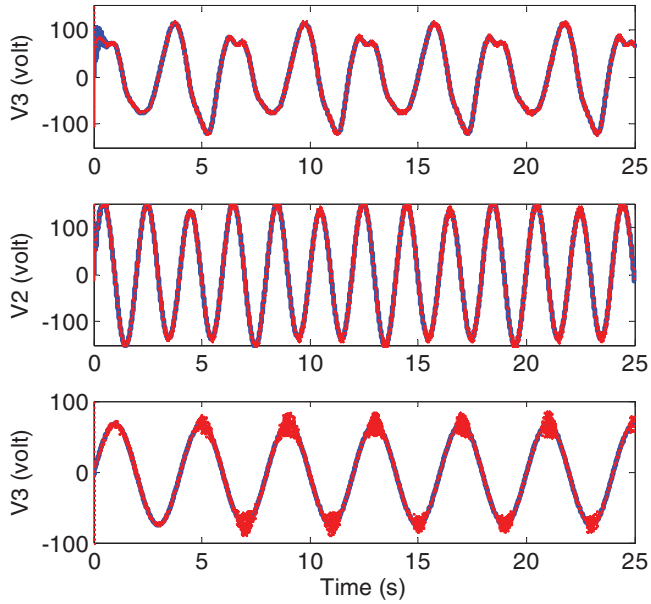


Fig. 14. Comparison of motor voltages (Fourier series : —, Neuro-fuzzy : - - -).

set to 10. The control law designed in Wai *et al.*[29] was applied to the robotic system described in this paper. The desired trajectory is defined in (68). In order to compare the performances of two controllers, motor voltages and tracking errors are illustrated in Figs. 14 and 15, respectively. According to Fig. 14, the control efforts are nearly the same. According to Fig. 15, the tracking errors for the neuro-fuzzy controller are bounded. However, the tracking errors for the proposed method asymptotically converge to zero which indicates the proposed method superiority.

The performance of the proposed method in higher frequencies using the desired trajectory $\mathbf{q_d} = [\,1 - \cos(4\pi t/3)\;\; 1 - \cos(4\pi t/3)\;\; 1 - \cos(4\pi t/4)\,]^T$ was evaluated. All the controller parameters are the same as previous simulations. Just the fundamental period duration of Fourier series has been modified. The same trajectory has been applied to the neuro-fuzzy controller for comparison. The tracking errors are illustrated in Fig. 16 and the control efforts are presented in Fig. 17. As shown

https://doi.org/10.1017/S026357471500051X Published online by Cambridge University Press

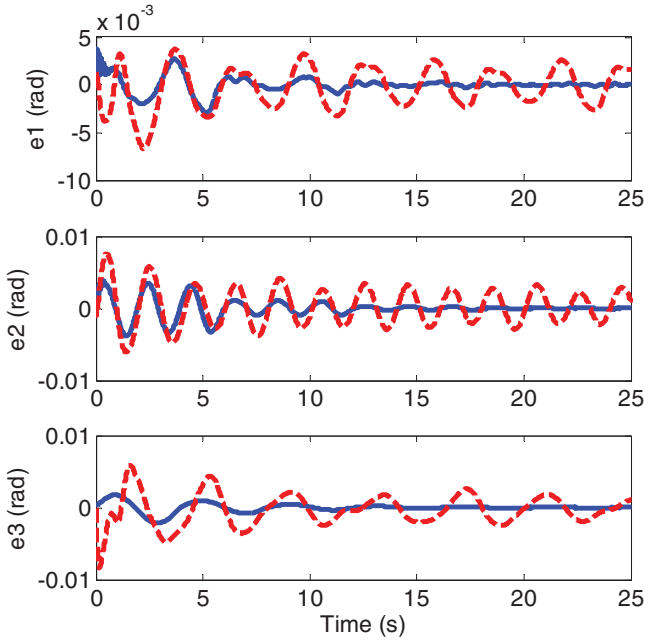


Fig. 15. Comparison of tracking errors (Fourier series : —, Neuro-fuzzy : - - -).

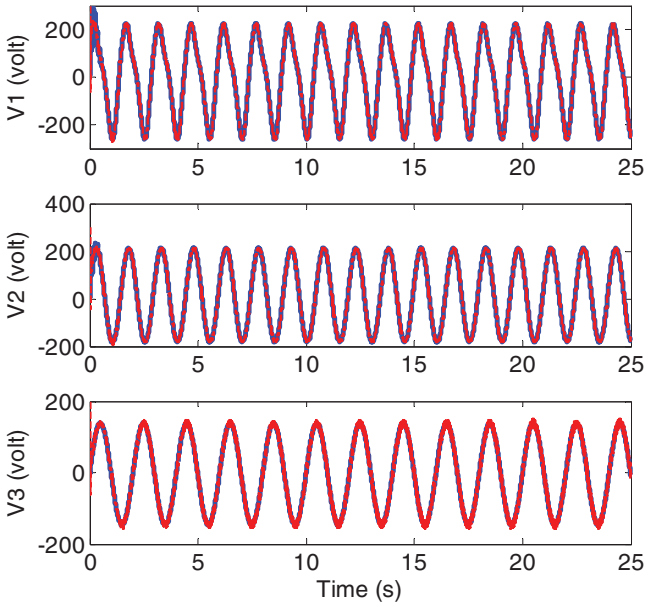


Fig. 16. Comparison of motor voltages in a higher frequency (Fourier series : —, Neuro-fuzzy : - - -)

in Fig. 16, the tracking error for the proposed method asymptotically converges to zero, while the convergence rate of the tracking error in the neuro-fuzzy controller is too slow. We can increase the parameters K_a and K_b in the neuro-fuzzy controller to reduce the tracking error; however, it will result in the chattering phenomenon in the control efforts. Since the desired trajectory speed has been increased, motor voltages have also increased, as shown in Fig. 17.

It is important to note that the proposed method is faster, since its computational load is less. In numerical simulations, it takes more than 15 min for the neuro-fuzzy program to run, while the proposed method needs less than 2 min.

https://doi.org/10.1017/S026357471500051X Published online by Cambridge University Press

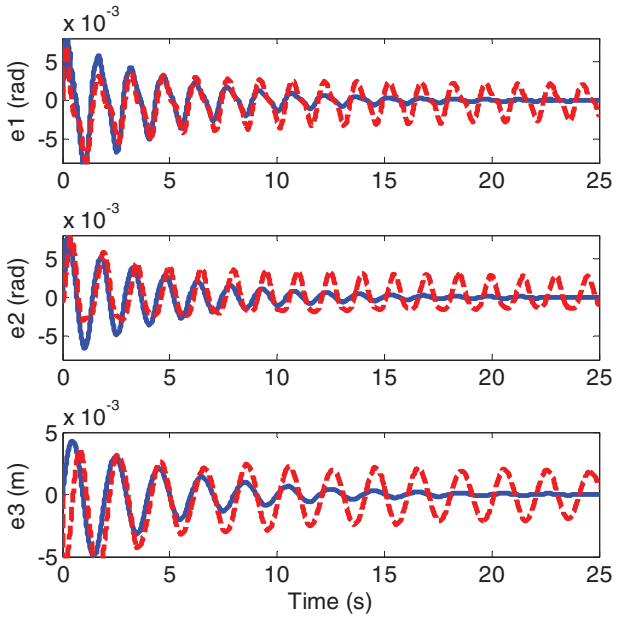


Fig. 17. Comparison of tracking errors in a higher frequency (Fourier series : —, Neuro-fuzzy : - - -).

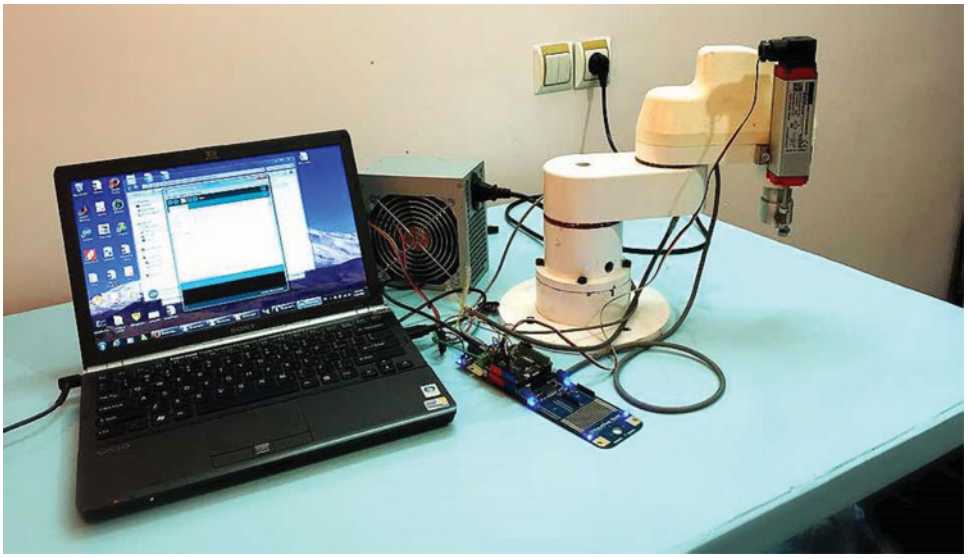


Fig. 18. The experimental setup.

8. Experimental Results

To validate the proposed controller performance on a real robot manipulator, experimental results are presented in this section. A photograph of the practical control system is depicted in Fig. 18. Three geared DC servomotor are utilized as the actuators. The maximum permitted voltage for motors in the revolute joints and the prismatic joint are 5 and 12 V, respectively. The DFrobotshop Rover board which is an Arduino compatible dual motor driver based on ATmega328 has been considered for driving the motors in revolute joints. The third motor is driven using the DFrobot L298p Twin V1.1 motor shield. The proposed controller has been implemented using the Arduino programming environment and inserted to the DFrobotshop Rover board using the USB connection. In order to provide the controller with position feedbacks from revolute joints, the potentiometer terminals have been extracted from the motor boxes and connected to the analog inputs of the board. Also, as shown in Fig. 18, a linear potentiometer measures the linear displacement of the prismatic joint. The desired

https://doi.org/10.1017/S026357471500051X Published online by Cambridge University Press

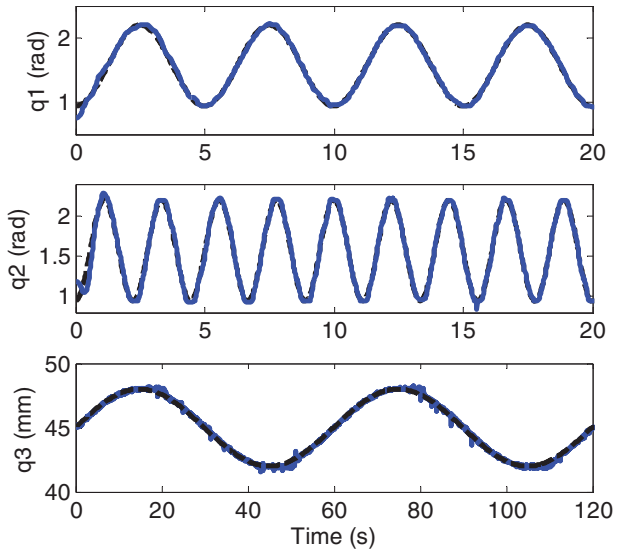


Fig. 19. Tracking performance for the real robot (desired trajectory : - - -, robot joint variable: —).

trajectory has been defined as

$$\mathbf{q_d} = \begin{bmatrix} (\pi/2) - (\pi/5)\cos(4\pi t/10)^{\text{rad}} \\ (\pi/2) - (\pi/5)\cos(9\pi t/10)^{\text{rad}} \\ 45 + 2.5\sin(\pi t/30)^{\text{mm}} \end{bmatrix} \tag{78}$$

The maximum angular displacement of the motors in joints 1 and 2 is about 200 (deg.) and the maximum linear displacement of the third joint is 8 cm. The desired trajectories were selected such that the robot moves at the middle of these ranges and the frequencies have been chosen with respect to the maximum permitted voltage of motors. In fact, the maximum frequencies that will not result in actuator saturation have been selected. The proposed controller given by (27) has been applied to the robotic system. The proportional gain $\mathbf{K_p}$ and the convergence rate γ have been set to 3500 and 1000, respectively. The parameter m in (67) has been set to 2. The data rate in bits per second (baud) for serial data transmission has been set to 38400. The tracking performances for different joints are illustrated in Fig. 19. According to these figures, the proposed model-free controller is robust against various uncertainties and can track the desired trajectories very well. Control efforts are plotted in Fig. 20. As shown in these figures, motor voltages are within the permitted range. Fourier series coefficients for the first joint are given in Fig. 21. As shown in this figure, these coefficients are bounded and converge to constant values. Although it takes more than 20 s for these coefficients to converge, the controller tracking performance is acceptable, even before this convergence.

In order to test the controller performance for other trajectories, square wave paths have been applied to this robot. According to Assumption 1, the desired trajectory should be differentiable. Therefore, some model references have been used to produce differentiable signals. The transfer function $G(s) = 6.25/(s^2 + 5s + 6.25)$ is selected for the first and second joints and $G(s) = 0.64/(s^2 + 1.6s + 0.64)$ is chosen for the third joint. The desired paths and robot response are illustrated in Fig. 22. According to this figure, the controller can track these square wave trajectories very well, without any overshoot. Motor voltages are presented in Fig. 23. As shown in this figure, the control efforts do not exceed the maximum permitted ranges and become smooth after some variations.

Although the real robot and motors are quite different from the described robot and motors in Tables II and III, there are some important common features between experimental and simulation results which imply a unique behavior of the controller for different robots.

1. The controller gains such as $\mathbf{K_p}$ and γ for both robots are relatively large.
2. Fourier series coefficients converge to constant values in both robots.

https://doi.org/10.1017/S026357471500051X Published online by Cambridge University Press

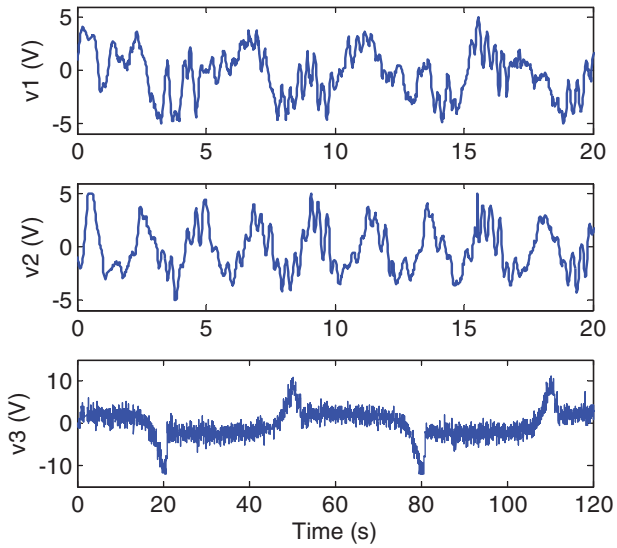


Fig. 20. Control efforts for the real robot.

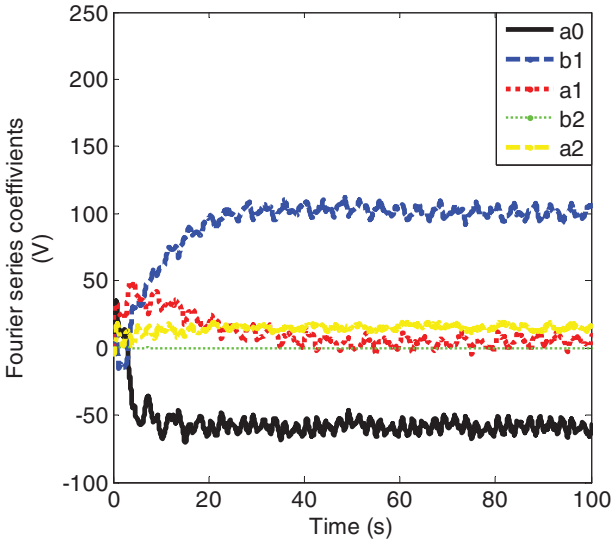


Fig. 21. Fourier series coefficients for the first joint of the real robot.

3. The time needed for coefficient convergence is large for both robots.
4. Before parameter convergence, both robots have acceptable tracking performances.
5. As shown in Figs. 5 and 23, when the desired path changes suddenly, motor voltages have fast variations and after that they become smooth.

9. Conclusion

Recently, some model-free control approaches have been presented in the literature for robust tracking control of robot manipulators. These approaches are based on uncertainty estimation using orthogonal functions such as Fourier series. However, the fundamental period duration of the Fourier series expansion has been left as an open problem. In this paper, it has been assumed that the desired trajectories are periodic functions, since they are very common in industry. Then, it has been intuitively shown that the least common multiples of the fundamental period durations of desired trajectories

https://doi.org/10.1017/S026357471500051X Published online by Cambridge University Press

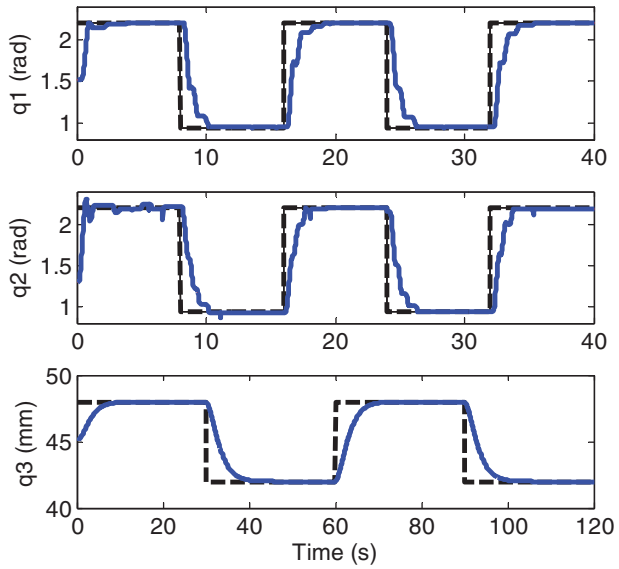


Fig. 22. Tracking performance of the real robot for square wave paths (desired trajectory : - - -, robot joint variable: —).

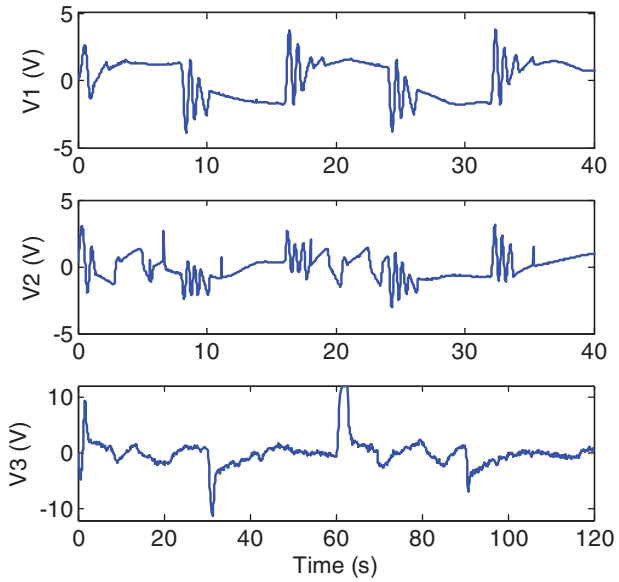


Fig. 23. Motor voltages in the real robot for square wave paths.

can be a proper selection for the fundamental period duration of the Fourier series expansion. The control law is designed based on the VCS using a model free control approach. The stability analysis guarantees that the tracking errors converge to zero asymptotically and all the state variables and the control effort are bounded. In comparison with previous regressor free approaches, the control design in this paper is much simpler and less computational, since just the lumped uncertainty is estimated in this paper. Simulation and experimental results verify that the proposed method can follow various trajectories with small tracking errors and acceptable control efforts.

References

1. Z. Qu and D. M. Dawson, *Robust Tracking Control of Robot Manipulators* (IEEE Press, Inc., New York, 1996).

https://doi.org/10.1017/S026357471500051X Published online by Cambridge University Press

2. H. G. Sage, M. F. De Mathelin and E. Ostertag, "Robust control of robot manipulators: A survey," *Int. J. Control* **72**(16), 1498–1522 (1999).
3. C. Abdallah, D. Dawson, P. Dorato and M. Jamshidi, "Survey of robust control for rigid robots," *IEEE Control Syst. Mag*. **11**, 24–30 (1991).
4. M. J. Corless, "Control of uncertain nonlinear systems," *ASME Trans. J. Dyn. Syst. Meas. Control* **115**(2B), 362–372 (1993).
5. M. M. Fateh, "Proper uncertainty bound parameter to robust control of electrical manipulators using nominal model," *Nonlinear Dyn.* **61**(4), 655–666 (2010).
6. M. M. Fateh and S. Khorashadizadeh, "Optimal Robust voltage control of electrically driven robots," *Nonlinear Dyn*. **70**, 1445–1458 (2012).
7. S. Nicosia and P. Tomei, "Robot control by using only joint position measurements," *IEEE Trans. Autom. Control* **35**(9), 1058–1061 (1990).
8. S. E. Talole, J. P. Kolhe and S. B. Phadke, "Extended-state-observer-based control of flexible-joint system with experimental validation," *IEEE Trans. Ind. Electron.* **57**(4), 1411–1419 (2010).
9. W. H. Chen, D. J. Ballance, P. J. Gawthrop and J. O'Reilly, "A nonlinear disturbance observer for robotic manipulators," *IEEE Trans. Ind. Electron.* **47**(4), 932–938 (2000).
10. J. J. Slotine and W. Li, *Applied Nonlinear Control* (Prentice-Hall NJ, USA, 1991).
11. I. Uzmay and R. Burkan, "Parameter estimation and upper bounding adaptation in adaptive-robust control approaches for trajectory control of robots," *Robotica* **20**(6), 653–660 (2002).
12. R. Garcia-Hernandez, E. Sanchez, E. Bayro-Corrochano, V. Santibanez and J. Ruz-Hernandez, "Real-time decentralized neural block control: Application to a two DOF robot manipulator," *Int. J. Innovative Comput. Inf. Control* **7**(3), 1075–1085 (2011).
13. J. Peng, J. Wang and Y. Wang, "Neural network based robust hybrid control for robotic system: An H $_\infty$ approach," *Nonlinear Dyn*. **65**, 421–431 (2011).
14. S. Puga-Guzmán, J. Moreno-Valenzuela and V. Santibáñez, "Adaptive neural network motion control of manipulators with experimental evaluations," *Sci. World J.* **2014**, 1–13. doi: 10.1155/2014/694706 (2014).
15. M. M. Fateh and S. Khorashadizadeh, "Robust control of electrically driven robots by adaptive fuzzy estimation of uncertainty," *Nonlinear Dyn.* **69**, 1465–1477 (2012).
16. M. M. Fateh, S. Azargoshasb and S. Khorashadizadeh, "Model-free discrete control for robot manipulators using a fuzzy estimator," *Int. J. Comput. Math. Electr. Electron. Eng.* **33**(3), 1051–1067, (2014).
17. L. X. Wang, *A Course in Fuzzy Systems and Control* (Prentice-Hall, New York, 1997).
18. M. M. Fateh, "On the voltage-based control of robot manipulators," *Int. J. Control. Autom. Syst.* **6**(5), 702–712 (2008).
19. J. Orrante-Sakanassi, V. Santibañez and J. Moreno-Valenzuela, "Stability analysis of a voltage-based controller for robot manipulators," *Int. J. Adv. Robot. Syst.* **10**, 1–19. doi: 10.5772/53894 (2013).
20. M. M. Fateh, "Nonlinear control of electrical flexible-joint robots," *Nonlinear Dyn*. **67**, 2549–2559 (2012).
21. S. Khorashadizadeh and M. M. Fateh, "Robust control of flexible-joint robots using voltage control strategy," *Nonlinear Dyn*. **67**, 1525–1537 (2012).
22. M. M. Fateh, "Robust voltage control of electrical manipulators in task-space," *Int. J. Innov. Comput. Info. Control* **6**(6), 2691–2700 (2010).
23. M. C. Chien and A. C. Huang, "Regressor-free Adaptive Impedance Control of Flexible-Joint Robots using FAT," *Proceedings of the 2006 American Control Conference*, (2006) pp. 3904–3909.
24. M. C. Chien and A. C. Huang, "Adaptive impedance controller design for flexible-joint electrically-driven robots without computation of the regressor matrix," *Robotica* **30**, 133–144 (2012).
25. E. Kreyszig, *Advanced Engineering Mathematics* (John Wiley & Sons, 2007).
26. M. W. Spong, S. Hutchinson and M. Vidyasagar, *Robot Modelling and Control* (Wiley, Hoboken, 2006).
27. G. H. Hardy and E. M. Wright, *An Introduction to the Theory of Numbers* (Oxford University Press, 1979).
28. S. Khorashadizadeh and M. M. Fateh, "Robust task-space control of robot manipulators using Legendre polynomials for uncertainty estimation," *Nonlinear Dyn*. **79**(2), 1151–1161 (2014), DOI: 10.1007/s11071-014-1730-5.
29. R. J. Wai and P. C. Chen, "Intelligent tracking control for robot manipulator including actuator dynamics via TSK-type fuzzy neural network," *IEEE Trans. Fuzzy Systs.* **12**(4), 552–559 (2004).

Appendix 1

Proof of Lemma 1: We can write $a = 2^n a_0$ and $b = 2^m b_0$ in which n and m are integer numbers and 2 is not included in prime factorization of a_0 and b_0. Therefore,

$$(a, b) = 2^{\min(n,m)} \times (a_0, b_0) = W_1 \times (a_0, b_0) \tag{79}$$

The following three cases can be considered for n: $n = 0, n = n_1$ and $n = -n_1$ where n_1 is a positive integer number. The same cases can be considered for m: $m = 0, m = m_1$ and $m = -m_1$ where m_1 is a positive integer number. Thus, there are 9 possible cases for $(2a, b)$. By investigating these 9 cases we can verify **Lemma 1**.

https://doi.org/10.1017/S026357471500051X Published online by Cambridge University Press

The power of 2 in (a, b) is given by $\min(n, m)$. When a is multiplied by 2, the power of 2 in $(2a, b)$ is given by $\min(n + 1, m)$. Thus, we can generally conclude that:

$$(2a, b) = 2^{\min(n+1,m)} \times (a_0, b_0) = W_2 \times (a_0, b_0) \tag{80}$$

For example consider the case $n = 0$ and $m = 0$. We can write $W_1 = 2^{\min(0,0)} = 1$ and $W_2 = 2^{\min(1,0)} = 1$. Thus, $(2a, b) = (a, b)$.

If $n = 0$ and $m = m_1$, we have $W_1 = 2^{\min(0,m_1)} = 1$ and $W_2 = 2^{\min(1,m_1)}$. Since $m_1 \geq 1$, one can easily obtain $W_2 = 2$. As a result, $(2a, b) = 2(a, b)$.

If $n = 0$ and $m = -m_1$, we have $W_1 = 2^{\min(0,-m_1)} = 2^{-m_1}$ and $W_2 = 2^{\min(1,-m_1)} = 2^{-m_1}$. Therefore, $(2a, b) = (a, b)$.

If $n = n_1$ and $m = 0$, we have $W_1 = 2^{\min(n_1,0)} = 1$ and $W_2 = 2^{\min(n_1+1,0)} = 1$. As a result, $(2a, b) = (a, b)$.

If $n = n_1$ and $m = m_1$, the following 3 cases are possible: $n_1 > m_1$, $n_1 = m_1$ and $n_1 < m_1$. Consider the case $n_1 > m_1$. We have $W_1 = 2^{\min(n_1, m_1)} = 2^{m_1}$ and $W_2 = 2^{\min(n_1+1, m_1)} = 2^{m_1}$. As a result, $(2a, b) = (a, b)$. Now, suppose that $n_1 = m_1$. Therefore, $W_1 = 2^{\min(n_1, m_1)} = 2^{m_1}$ and $W_2 = 2^{\min(n_1+1, m_1)} = 2^{m_1}$ which obtains $(2a, b) = (a, b)$. In the case $n_1 < m_1$, $W_1 = 2^{\min(n_1, m_1)} = 2^{n_1}$. Since n_1 and m_1 are integer numbers, $n_1 + 1 = m_1$ or $n_1 + 1 < m_1$. Thus, $W_2 = 2^{\min(n_1+1, m_1)} = 2^{n_1+1}$ which obtains $(2a, b) = 2(a, b)$.

Similarly, we can discuss other cases and verify **Lemma 1**.

Appendix 2

Proof of Lemma 2: The fundamental period duration of $y(t)$ is the least T that satisfies $y(t + T) = y(t)$. Therefore, we should have

$$\cos\left(\frac{2\pi}{T_1}(t+T)+\alpha_1\right) \pm \sin\left(\frac{2\pi}{T_2}(t+T)+\alpha_2\right) = \cos\left(\frac{2\pi}{T_1}t+\alpha_1\right) \pm \sin\left(\frac{2\pi}{T_2}t+\alpha_2\right) \tag{81}$$

If integer numbers k_1 and k_2 exist so that $\frac{2\pi}{T_1}T = 2k_1\pi$ and $\frac{2\pi}{T_2}T = 2k_2\pi$, then (81) will be satisfied. In other words, we should find the least T such that $T = k_1T_1 = k_2T_2$. Thus, T is the least common multiple of T_1 and T_2.

Appendix 3

Proof of Lemma 3: Using sinusoidal unities, $x(t)$ in (50) can be expressed by

$$x(t) = \frac{1}{2}\left[\sin\left(\frac{2\pi}{T_1}t - \frac{2\pi}{T_2}t + \alpha_1 - \alpha_2\right) + \sin\left(\frac{2\pi}{T_1}t + \frac{2\pi}{T_2}t + \alpha_1 + \alpha_2\right)\right] \tag{82}$$

which can be simplified as

$$x(t) = \frac{1}{2}\left[\sin\left(\frac{2\pi}{T_a}t + \alpha_1 - \alpha_2\right) + \sin\left(\frac{2\pi}{T_b}t + \alpha_1 + \alpha_2\right)\right] \tag{83}$$

where $T_a = \frac{T_1T_2}{|T_1-T_2|}$ and $T_b = \frac{T_1T_2}{T_1+T_2}$. Without loss of generality, we can assume that $T_1 > T_2$. The case $T_2 > T_1$ can be similarly proven. According to **Lemma 1**, the fundamental period duration of $x(t)$ is given by

$$T_x = [T_a, T_b] = T_1T_2\left[\frac{1}{T_1 - T_2}, \frac{1}{T_1 + T_2}\right] \tag{84}$$

Using (45), one can easily obtain

$$T_x = \frac{T_1T_2}{(T_1 - T_2, T_1 + T_2)} \tag{85}$$

https://doi.org/10.1017/S026357471500051X Published online by Cambridge University Press

According to (44), we can write

$$T_x = \frac{T_1 T_2}{(2T_1, T_1 + T_2)} \tag{86}$$

It seems that in order to prove **Lemma 3**, we should find a relation between (T_1, T_2) and $(2T_1, T_1 + T_2)$. Assume that $(T_1, T_2) = T_0$. Using (44), it can be concluded that $(T_1, T_1 + T_2) = T_0$. According to **Lemma 1**, $(2T_1, T_1 + T_2) = T_0$ or $(2T_1, T_1 + T_2) = 2T_0$. Therefore, T_x in (85) is given by $[T_1, T_2]$ or $[T_1, T_2]/2$.

Appendix 4

Proof of Lemma 4: First, consider that

$$\left[\frac{a}{2}, b\right] = \frac{[a, b]}{M} \tag{87}$$

where a and $b$belong to positive rational numbers and $M \in \{1, 2\}$. Similar to the proof in **Appendix 1**, one can easily verify (87). Now, suppose that in **Lemma 4** we have $j = 3$. Thus,

$$x(t) = \cos\left(\frac{2\pi}{T_1}t + \alpha_1\right) \times \sin\left(\frac{2\pi}{T_2}t + \alpha_2\right) \times \cos\left(\frac{2\pi}{T_3}t + \alpha_3\right) \tag{88}$$

We can write (88) as

$$x(t) = x_0(t) \times \cos\left(\frac{2\pi}{T_3}t + \alpha_3\right) \tag{89}$$

in which $x_0(t) = \cos(\frac{2\pi}{T_1}t + \alpha_1) \times \sin(\frac{2\pi}{T_2}t + \alpha_2)$ is a periodic function. According to **Lemma 3**, its fundamental period duration is given by $T_0 = [T_1, T_2]/K$ where K belongs to the set $\{1, 2\}$. Thus, $x_0(t)$ can be rewritten as

$$x_0(t) = \cos\left(\frac{2\pi}{T_0}t + \alpha_0\right) \tag{90}$$

Using **Lemma 2**, one can conclude that the fundamental period duration of $x(t)$ in (89) is given by $T_x = [T_0, T_3]/K'$ in which K' belongs to the set $\{1, 2\}$. In other words, we have

$$T_x = \left[\frac{[T_1, T_2]}{K}, T_3\right]/K' \tag{91}$$

In the case that $K = 1$, T_x in (91) is given by

$$T_x = \frac{[[T_1, T_2], T_3]}{K'} = \frac{[T_1, T_2, T_3]}{K'} \tag{92}$$

where $K' \in \{1, 2\}$. Now, assume that $K = 2$. According to (87), T_x in (91) can be rewritten as

$$T_x = \frac{[[T_1, T_2], T_3]}{MK'} \tag{93}$$

where $M \in \{1, 2\}$. Using (92) and (93), we can write

$$T_x = \frac{[T_1, T_2, T_3]}{K''} \tag{94}$$

where $K'' \in \{1, 2, 4\}$. Therefore, one can easily extend this result to the cases where $j > 3$ and verify **Lemma 4**.

https://doi.org/10.1017/S026357471500051X Published online by Cambridge University Press